Assessing origins of end-Triassic tholeiites from Eastern North America using hafnium isotopes

Lynne J Elkins[1,1], Christine Marie Meyzen[2,2], Sara Callegaro[3,3], Andrea Marzoli[4,4], and Michael Bizimis[5,5]

[1]University of Nebraska-Lincoln
[2]Università degli Studi di Padova
[3]University of Oslo
[4]Dipartimento di Mineralogia e Petrologia, Universita' di Padova
[5]University of South Carolina

November 30, 2022

Abstract

The driving processes responsible for producing the Central Atlantic Magmatic Province, the Large Igneous Province associated with end-Triassic rifting of Pangea, remain largely debated. Because their compositions encompass most of the Central Atlantic basalt spectrum, tholeiites from southern Eastern North America are considered pivotal for identifying magma origins. New 176Hf/177Hf measurements for 201 Ma Eastern North American tholeiites dominantly record a local petrogenetic history. Their εHf ratios, corrected to an emplacement age of 201 Ma (-7.85 to +5.86), form a positive but shallowly sloped array slightly deviating from the terrestrial array on a εHf vs. εNd diagram. Comparison of 176Hf/177Hf to other isotope ratios and trace elements helps to rule out several petrogenetic scenarios, particularly mixing of melts from global depleted or enriched mantle components. In contrast, partial melting of subduction-metasomatized mantle can explain the parental magma composition for southern Eastern North America. Such metasomatism likely occurred during Paleozoic subduction around Pangea and may have been dominated by sediment-derived fluid reactions. The observed 176Hf/177Hf vs. 143Nd/144Nd array may reflect subsequent assimilation of lower continental crust, perhaps together with limited direct melting of recycled continental crust in the asthenosphere. The proposed recycling scenario does not specifically support or preclude a mantle plume origin for the Central Atlantic Magmatic Province, but instead points toward the presence of a distinct local mantle source and crustal assimilation processes during magma transport. Detailed understanding of these local effects is needed in order to more accurately understand the origins of Large Igneous Provinces.

Assessing origins of end-Triassic tholeiites from Eastern North America using hafnium isotopes

Lynne J. Elkins[1,] *, Christine M. Meyzen[2], Sara Callegaro[3], Andrea Marzoli[2], Michael Bizimis[4]

[1] University of Nebraska-Lincoln, Lincoln, NE 68510; lelkins@unl.edu

[2] Dipartimento di Geoscienze, Università degli Studi di Padova, Via G. Gradenigo, 6, 35131 Padova, Italy; andrea.marzoli@unipd.it, christine.meyzen@unipd.it

[3] Centre for Earth Evolution and Dynamics, University of Oslo, Oslo, Norway; sara.callegaro@geo.uio.no

[4] University of South Carolina; mbizimis@geol.sc.edu

* Corresponding author: Lynne Elkins (lelkins@unl.edu)

Key Points:

- End-Triassic tholeiites from Eastern North America were likely products of melting Paleozoic age, subduction-metasomatized mantle
- Direct melting of recycled crustal rocks may also have occurred, but cannot fully explain the tholeiite isotopic compositions observed
- Southern Eastern North American tholeiites likely also experienced assimilation of lower continental crust, possibly intermediate granulite

Abstract

The driving processes responsible for producing the Central Atlantic Magmatic Province, the Large Igneous Province associated with end-Triassic rifting of Pangea, remain largely debated. Because their compositions encompass most of the Central Atlantic basalt spectrum, tholeiites from southern Eastern North America are considered pivotal for identifying magma origins. New $^{176}Hf/^{177}Hf$ measurements for 201 Ma Eastern North American tholeiites dominantly record a local petrogenetic history. Their ε_{Hf} ratios, corrected to an emplacement age of 201 Ma (-7.85 to +5.86), form a positive but shallowly sloped array slightly deviating from the terrestrial array on a ε_{Hf} vs. ε_{Nd} diagram. Comparison of $^{176}Hf/^{177}Hf$ to other isotope ratios and trace elements helps to rule out several petrogenetic scenarios, particularly mixing of melts from global depleted or enriched mantle components. In contrast, partial melting of subduction-metasomatized mantle can explain the parental magma composition for southern Eastern North America. Such metasomatism likely occurred during Paleozoic subduction around Pangea and may have been dominated by sediment-derived fluid reactions. The observed $^{176}Hf/^{177}Hf$ vs. $^{143}Nd/^{144}Nd$ array may reflect subsequent assimilation of lower continental crust, perhaps together with limited direct melting of recycled continental crust in the asthenosphere. The proposed recycling scenario does not specifically support or preclude a mantle plume origin for the Central Atlantic Magmatic Province, but instead points toward the presence of a distinct local mantle source and crustal assimilation processes during magma transport. Detailed understanding of these local effects is needed in order to more accurately understand the origins of Large Igneous Provinces.

Key words: 8410 Geochemical modeling; 8137 Hotspots, large igneous provinces, and flood basalt volcanism; 1040 Radiogenic isotope geochemistry; 1037 Magma genesis and partial

56 melting

1. INTRODUCTION

The Triassic-Jurassic rifting of Pangea and subsequent opening of the central Atlantic Ocean represent a major stage of a Wilson cycle, describing the formation and destruction of oceanic basins and supercontinents (Wilson, 1966). Wilson's classic model drew directly on the central Atlantic basin and its history of repeated closures and reopenings as a primary example of global tectonic processes. End-Triassic rifting was associated with the emplacement of one of the most voluminous continental flood basalt provinces in Earth history (Figure 1), the Central Atlantic Magmatic Province (CAMP; Marzoli et al., 1999), an event significant enough to have likely triggered the end-Triassic mass extinction (Capriolo et al., 2020; Cirilli et al., 2009; Davies et al., 2017; Heimdal et al., 2018; Hesselbo et al., 2002; Marzoli et al., 2004). Major continental rifting events in geologic history are commonly associated with the eruption of a large igneous province (LIP), but the causal relationships linking rifts with LIPs remain unclear. The distinction and the transition between passive and active rifting models has been the object of several studies (Burov & Gerya, 2014; Courtillot et al., 1999; Koptev et al., 2015; Sengör & Burke, 1978), all seeking to better understand what processes initiate rifting and what factors cause rifted margins to be magma-rich or magma-poor (Gillard et al., 2017). Large igneous provinces may also record the arrival of deep-seated mantle plumes at the base of the lithosphere, which could in turn act to initiate rifting, but it has been difficult to fully reconcile plume head arrival with continental rifting models in all settings (e.g., Carlson, 1991; Courtillot et al., 1999; Morgan, 1983; Saunders et al., 2007).

One peculiarity of CAMP magmas is that they display an overall high degree of geochemical heterogeneity, which has led researchers to propose diverse magma origins such as an upwelling mantle plume (e.g., Cebriá et al., 2003; De Boer, 1992; Oyarzun et al., 1997; Wilson, 1997);

metasomatized subcontinental lithospheric mantle (SCLM) (e.g., Deckart et al., 2005; Merle et al., 2011; Verati et al., 2005); and asthenosphere and/or SCLM modified by subduction-derived materials (e.g., Alibert, 1985; Callegaro et al., 2013, 2017; Dorais et al., 2005; Dupuy et al., 1988; Heatherington & Mueller, 1999; Marzoli et al., 2019; Merle et al., 2014; Pegram, 1990; Whalen et al., 2015). These proposed origins have been likewise interpreted to indicate various geodynamic scenarios (e.g., Marzoli et al., 2018, and references therein). As an additional source of complexity, while some of the diverse magma types have been identified across the province, other CAMP magma compositions vary from region to region (Marzoli et al., 2018). It remains unclear whether these regional heterogeneities are derived from locally diverse asthenospheric or continental lithospheric mantle sources, or inherited by assimilation of local continental lithosphere by deeper, perhaps plume-derived primary magmas. Each scenario has distinct implications for how end-Triassic rifting and associated LIP emplacement occurred. The diversity of models further demonstrates the uncertainty about the origins of LIPs and their links to continental rifts.

As an important component of this ongoing effort to understand the origins of CAMP, much prior literature has been dedicated to the petrogenesis of CAMP basalts from Eastern North America (ENA), but questions persist about the characteristics and origins of their primary melt sources, and the role and importance of assimilation and crustal contamination in modifying primitive melt compositions (e.g., Callegaro et al., 2013; Dorais & Tubrett, 2008; Dostal and Dupuy, 1984; Dostal & Durning, 1998; Heatherington & Mueller, 1999; McHone, 2000; Merle et al., 2014; Pegram, 1990; Puffer, 1992, 2001, 2003; Shellnutt et al., 2018; Tollo & Gottfried, 1992; Whalen et al., 2015). Because of the geochemical heterogeneity recorded by the tholeiites from Georgia to Virginia in the southern part of ENA, which encompass most of the CAMP

geochemical spectrum, and taking advantage of the mineralogical sensitivity of the ^{176}Lu-^{176}Hf isotopic system with respect to clinopyroxene-garnet ratios, this study aims to place new constraints on the formation of CAMP and of LIPs more generally.

2. GEOLOGIC SETTING

2.1. Tectonic setting of CAMP

The opening of the Central Atlantic oceanic basin started with end-Triassic rifting of the supercontinent Pangea, an event associated with the regional emplacement of tholeiitic magmas over an estimated total surface of 10^7 km^2 spanning present-day eastern North America, northern South America, northwest Africa, and southwestern Europe (Figure 1) (Marzoli et al., 1999, 2018). Central Atlantic Magmatic Province emplacement occurred at ~201 Ma with a duration of peak magmatic activity constrained to less than 0.6 Ma (e.g., Blackburn et al., 2013; Davies et al., 2017; Deckart et al., 1997; Dunning & Hodych, 1990; Hames et al., 2000; Hodych & Dunning, 1992; Jourdan et al., 2009; Knight et al., 2004; Marzoli et al., 2004, 2011, 2019; Nomade et al., 2007; Sebai et al., 1991; Verati et al., 2005, 2007). At ca. 201.6 to 200.9 Ma, several short-lived magmatic pulses occurred all over the CAMP and preceded continental break-up by several million years (Blackburn et al., 2013; Davies et al., 2017; Knight et al., 2004).

2.2. Models for CAMP formation

The origins of LIPs and their relationship with continental rifting are subjects of long standing debate (e.g., Bryan & Ernst, 2008; Carlson, 1991; Coffin & Eldholm, 1992; Kent, 1991; Morgan, 1983; Saunders et al., 2007). Many studies have invoked one or more mantle plumes as triggering mechanisms for CAMP rifting and magmatism, invoking heat-driven lithospheric

erosion and thinning, wide-scale asthenospheric upwelling and melting in a plume head, broad crustal magmatic emplacement, and possible localized focusing of regional extension in response to plume impingement on the overlying plate (e.g., Cebriá et al., 2003; Hill, 1991; Lizarralde & Holbrook, 1997; McHone, 1978; Morgan, 1983; Oyarzun et al., 1997; Ruiz-Martínez et al., 2012; White & McKenzie, 1989; Wilson, 1997).

However, plume evidence related to the CAMP episode is ambiguous: the central Atlantic basin does not include any hotspot tracks of early Jurassic age, and dike orientations and the near-synchronous onset of magmatism from Bolivia to Spain are inconsistent with a centralized, radiating plume impact (e.g., Davies et al., 2017; May, 1971; McHone, 2000; Verati et al., 2005). Therefore, many studies have advocated for non-plume dynamical mechanisms for triggering rifting and melting (e.g., Bédard, 1992; De Min et al., 2003; Holbrook & Kelemen, 1993; Holbrook et al., 1994; Kontak, 2008; McHone, 2000). These alternative models for CAMP invoke other melt generation mechanisms, such as subcontinental insulation heating and edge-driven convection (e.g., Anderson, 1994; Coltice et al., 2007).

Geochemically, most CAMP magmas exhibit signatures enriched in incompatible trace elements, with combined Pb-Sr-Nd-Os radiogenic isotopes indicating the involvement of one or more long-lived source reservoirs with time-integrated incompatible trace element enrichment (e.g., Callegaro et al., 2013, 2014, 2017; Marzoli et al., 2019; Merle et al., 2011, 2014; Whalen et al., 2015). While these geochemical patterns could indicate melt contributions from recycled material entrained in a deep mantle plume, geochemical signatures such as LILE enrichments and Nb depletions in CAMP are notably arc-like (e.g., De Min et al., 2003; Deckart et al., 2005; Jourdan et al., 2003; Puffer, 2001).

The arc-like trace element signatures observed in CAMP magmas could indicate a unique local mantle source composition, or may be derived from assimilation of continental lithosphere during magma transport (Alibert, 1985; Bertrand, 1991; Bertrand et al., 1982; Cebriá et al., 2003; Chabou et al., 2010; De Min et al., 2003; Deckart et al., 2005; Dupuy et al., 1988; Heatherington & Mueller, 1999; Iacumin et al., 2003; Jourdan et al., 2003; Papezik et al., 1988; Pegram, 1990; Puffer, 1992; Ragland et al., 1992; Tollo & Gottfried, 1992; Verati et al., 2005). A plume origin for the Sr-Nd-Pb isotope systematics of CAMP is likewise problematic given the lack of Atlantic OIBs with comparable signatures (e.g., Janney & Castillo, 2001; Pegram, 1990). A lack of primitive (picritic) magmas in CAMP is a hindrance when defining the mantle source origins for the LIP, but recent isotope analyses of ENA tholeiites suggest that for the least evolved magmas, a SCLM or shallow asthenospheric mantle source modified by either subduction-derived fluids or direct addition of subducted and/or delaminated continental crustal material is a viable scenario (Callegaro et al., 2013, 2014; Merle et al., 2014; Shelnutt et al., 2018; Whalen et al., 2015).

2.3. The Eastern North America study area

Eastern North American CAMP (Figure 1) hosts a particularly well-documented volcanic and intrusive tholeiite series, including dike swarms, sills, and basaltic flows exposed from Georgia (USA) to Newfoundland (Canada). The ENA series incorporate much of the observed geochemical diversity of the overall province. The major CAMP lava piles are locally associated with extensional grabens and half-grabens along what is now eastern North America. The Hartford-Newark-Gettysburg-Culpeper basins of Massachusetts, Connecticut, New Jersey, Pennsylvania, and Virginia host a series of three major volcanic episodes, including the oldest Orange Mountain series, the intermediate-age Preakness series, and the youngest Hook Mountain

series (e.g., Puffer, 1992; Tollo & Gottfried, 1992). These units are matched by similarly dated and geochemically identified basalts and feeder dikes in Canada (e.g., Kontak, 2008; Jourdan et al., 2009; Pe-Piper & Piper, 1999) and Morocco (e.g., Bertrand et al., 1982; Marzoli et al., 2019). Contrary to observations in Morocco and northern ENA, rift basins in southern Virginia, the Carolinas, and Georgia do not preserve lava flows and are dominated instead by diabase dikes and a few sills (e.g., Ragland et al., 1992; Weigand & Ragland, 1970).

Diabases and basalt flows from ENA are geochemically diverse, and detailed analysis has indicated that multiple parental magmas with distinct differentiation, fractionation, and/or assimilation paths are likely necessary to generate the geochemical variations observed (e.g., Tollo & Gottfried, 1992). Mantle potential temperatures extrapolated from high-Fo (> Fo_{87}) olivine cores from these rocks have a maximum calculated value of 1480ºC (Callegaro et al., 2013; Herzberg & Gazel, 2009; Hole, 2015), well below anomalously high temperatures calculated for the likely plume-related Deccan and Siberian LIPs, but at least 100 °C higher than normal ambient upper mantle (Herzberg & Gazel, 2009; Sobolev et al., 2011). These moderately high temperatures raise questions about the origins of that heat in the absence of a mantle plume; one possibility is continental insulation beneath supercontinents (e.g., Coltice et al., 2007; Rey, 2015). Within this framework, the wide geochemical variability observed in ENA tholeiitic dikes and sills makes it a particularly good focus region for placing new geochemical constraints on the diversity of magma source origins and the process of continental flood basalt production during rifting.

2. METHODS

2.1. CAMP sample selection and preparation

Tholeiitic basalt and diabase samples were selected to achieve a representative coverage across the geochemical variability observed in trace elements and Sr-Nd-Pb isotopes for the southern ENA region (12 samples), as well as targeted comparison to other regions within CAMP including the northern ENA Newark basin (six samples), Sierra Leone (one sample), and Morocco (one sample) (Table 1, Figure 1). The selected samples have relatively fresh, unaltered appearances, with prior major and trace element results indicative of minimal crustal assimilation or post-eruptive alteration (Callegaro et al., 2013, 2017; Marzoli et al., 2019; Merle et al., 2014). Of these, two southern ENA samples (CS28 and CS57) were selected because they are particularly Mg-rich (> 12 wt.% MgO) and are among the most primitive rocks ever recovered from CAMP (Table 1; Callegaro et al., 2013). An exception to the above criteria is sample NEW68 from the Preakness unit of the Newark Basin, which was selected because it is likely crustally contaminated (Merle et al., 2014).

The samples analyzed for this study were all collected during prior research, and sampling locations and previous geochemical measurements have been published elsewhere (Callegaro et al., 2013, 2017; Marzoli et al., 2019; Merle et al., 2014) (Table 1). Prior to analysis for the current study, any weathered rinds were removed by cutting with a trim saw. Fresh, visibly unaltered material was then broken into finer pieces using a rock hammer, which was protected with layers of clean plastic sheeting to prevent contamination. Sample material was then reduced to small chips and powdered using an agate mortar and pestle. Larger samples with a sufficient volume of material were further powdered using a Spex Shatterbox alumina grinding apparatus. Samples were prepared in this manner either at the University of Padova or at the University of Nebraska-Lincoln.

2.2. Analytical methods

Samples were analyzed for Hf isotopes in the Center for Elemental Mass Spectrometry, School of Earth, Ocean, and Environment, University of South Carolina. An aliquot of 100 mg of rock powder was weighed and digested in a Teflon-distilled HF:HNO_3 mixture in a 3:1 ratio. After dissolution, the solution was dried repeatedly in 6N HCl, after which Hf was separated from matrix elements using Eichrom LN-Spec Resin and methods after Munker et al. (2001). Hafnium separates were analyzed by mass spectrometry methods using a Thermo Neptune multi-collector inductively-coupled plasma mass spectrometer (MC-ICP-MS). Procedural blanks recorded Hf concentrations under 50 pg, and analytical precision was within 0.0017% (2σ standard error) for all measured samples (Table 2). Isotope compositions were corrected for mass fractionation using $^{179}Hf/^{177}Hf = 0.7325$. The JMC-475 standard was determined to have $^{176}Hf/^{177}Hf = 0.282152 \pm 0.000004$ (n = 10) for the first round of analyses and $^{176}Hf/^{177}Hf = 0.282142 \pm 0.000007$ (n = 10) for the second batch (Table 2). The data were corrected for instrumental bias using a JMC-475 reference value of 0.282160. As an additional test of external reproducibility, we analyzed a gabbroic sample from the Freetown Layered Complex (Sierra Leone) as a replicate of an earlier measurement by Callegaro et al. (2017), using a separate dissolution. Our newly measured $^{176}Hf/^{177}Hf$ ratio for this sample (0.282917 ± 0.000005; Table 2) is similar to the prior published result (0.282937 ± 0.000012). The two results are slightly outside of 2σ uncertainty with each other, however, which may be attributed to minor sample heterogeneity and the measurement of separate sample dissolutions. Additional analytical details and standard information can be found in Khanna et al. (2014), Mallick et al. (2015), and Frisby et al. (2016).

3. RESULTS

All data measured in this study have been age corrected to a crystallization age of 201 Ma using Lu/Hf ratios previously published for these samples (Callegaro et al., 2013, 2017; Marzoli et al., 2019; Merle et al., 2014) (Table 2); age-corrected isotopic ratios are hereafter indicated with "201 Ma" notation. A conservative uncertainty of ~5% for the Lu/Hf ratio translates to less than 0.3 ε_{Hf} units of uncertainty in the initial isotopic composition for rocks of this age, and has no effect on the conclusions of this study. Most samples from the southern ENA region form a distinct array exhibiting a shallower slope (slope = 0.92 ± 0.12) than the terrestrial array (Vervoort et al., 2011), being slightly shifted toward higher $\varepsilon_{Hf\ 201Ma}$ ratios for a given $\varepsilon_{Nd\ 201Ma}$ value (Table 2, Figure 2a). A notable exception is sample CS73 from Virginia, which plots along the terrestrial array. The oblique trend relative to the terrestrial array defined by southern ENA samples resembles trends previously observed for basalts from Hawaii (Blichert-Toft et al., 1999; Salters et al., 2006) and the Karoo LIP (Jourdan et al., 2007) (Figure 2a). Southern ENA $\varepsilon_{Hf\ 201Ma}$ ratios also form a slightly positive correlation with $^{206}Pb/^{204}Pb_{201Ma}$ isotope ratios (Callegaro et al., 2013) (Figure 2b). The latitudinal $\varepsilon_{Hf\ 201Ma}$ profile between 34 and 37 °N shows a decreasing southward gradient (Figure S1) toward more enriched (less radiogenic) isotope ratios, with the exception of sample CS73.

In contrast with ENA samples, those from the Newark basin, Morocco, and Sierra Leone are overall consistent with the global array (Vervoort et al., 2011) (Figure 2a). An exception is the sample NEW68, a Preakness unit tholeiite selected for comparison due to its distinct geochemical signature indicative of crustal assimilation (Merle et al., 2014); NEW68 has a slightly higher $\varepsilon_{Hf\ 201Ma}$ ratio for its $\varepsilon_{Nd\ 201Ma}$ than other Newark basin basalts. Newark basin samples exhibit a range of $\varepsilon_{Hf\ 201Ma}$ values from ~0 to +5 (Figure S1).

4. DISCUSSION

The shallow slope of southern ENA tholeiites relative to the terrestrial array (Figure 2a, Table 2) indicates a systematically increasing contribution from a low-ε_{Hf} source towards the south (Figure S1). However, unlike previous data sets such as Hawaiian basalts (Blichert-Toft et al., 1999; Salters et al., 2006) and the Karoo LIP (Jourdan et al., 2007), the southern ENA CAMP array extends towards low $^{206}Pb/^{204}Pb_{201Ma}$ ratios at the low-$\varepsilon_{Nd\ 201Ma}$ end of the array (Figure 2). Below, we explore a series of melt mixing and assimilation scenarios and compare the outcomes to the observed CAMP trace element and isotopic data, in an attempt to explain the origins of these isotopic characteristics.

4.1. Crustal assimilation in Carolina tholeiites

As noted above, aside from a few samples, recent isotopic studies of ENA and other CAMP rocks have indicated relatively minor crustal assimilation effects (up to 10% assimilation) in ENA tholeiites (Callegaro et al., 2013; Merle et al., 2014; Whalen et al., 2015), which have relatively low age-corrected $^{187}Os/^{188}Os_{201Ma}$ (0.128 – 0.187, mean 0.137) despite high $^{87}Sr/^{86}Sr_{201Ma}$ (0.70438 - 0.71074, mean 0.70613), high $^{207}Pb/^{204}Pb_{201Ma}$ (15.54 - 15.67, mean 15.61), variable $^{206}Pb/^{204}Pb_{201Ma}$ (17.41 - 18.65, mean 18.23), and low $^{143}Nd/^{144}Nd_{201Ma}$ ratios (0.51204 - 0.51251, mean 0.51230). However, due to a lack of Hf compositional and isotopic data for the potential end-member continental assimilants in the ENA province, it is unclear what effects up to 10% crustal assimilation may have had on the Hf isotope compositions of ENA CAMP magmas. To evaluate the potential impacts of assimilation on the Hf data set, we calculated the effects of assimilation-fractional crystallization on ENA basalts using energy-constrained methods after Bohrson and Spera (2001) and Spera and Bohrson (2001) (Tables S1,

S2; Figure 3), and considered three potential assimilants: local upper continental crust, and both mafic and intermediate-SiO_2, lower crustal granulite rocks. To simplify the scenarios tested, we make several initial assumptions, including the temperatures, compositions, and energy properties of the primary magma and three assimilants (see Tables S1, S2). Our calculations also assume a primary magma composition resembling the most incompatible element-depleted, southern ENA tholeiite measured in this study with respect to Hf (sample CS49, with low [Hf] = 1.3 ppm, high $\varepsilon_{Hf\ 201Ma}$ = +5.86) (Table 2).

To estimate the average composition of local upper continental crust, we used the mean compositions of measured Carolina terrane crustal rocks from Pettingill et al. (1984) and Sinha et al. (1996) and the data compilation of Whalen et al. (2015) (Table S1). The composition and age of the lower basement of the Carolina terrane is less well-constrained. In general, while some lower continental crust (LCC) may be Phanerozoic in age, many lower crustal rocks worldwide are composed of Archean to Proterozoic Precambrian granulites with a range of mafic to felsic compositions (e.g., Huang et al., 1995; Schmitz et al., 2004; Vervoort et al., 2000), and there is isotopic evidence that local Carolina terrane LCC is dominantly Proterozoic in age (Ingle et al., 2003). While a range of LCC ages is thus possible, here we focus on Proterozoic lower crustal sources for the Carolina terrane. Most lower crustal granulites measured lie along the terrestrial ε_{Nd}- ε_{Hf} array (Vervoort et al., 2000), but some granulite xenoliths exhibit decoupling of ε_{Hf} from ε_{Nd}, likely caused by the presence of cumulate or restite igneous minerals or by fractionation during metamorphic mineral growth (Schmitz et al., 2004). The decoupling toward higher ε_{Hf} relative to the terrestrial array is primarily observed in Proterozoic granulites (Huang et al., 1995; Schmitz et al., 2004; Zartman et al., 2013), and so also may play a role in the Carolina terrane (Ingle et al., 2003). As for major element compositions, while much of the LCC may be mafic,

Zhao and Guo (2019) and Guo et al. (2019) have observed that local Carolina LCC likely has an overall intermediate SiO_2 content; we thus test both mafic and intermediate-SiO_2 LCC compositions (Figure 3, Table S1). The mafic LCC composition used here resembles mafic granulite xenoliths from Michigan (Zartman et al., 2013) with decoupled ε_{Hf} and ε_{Nd}; alternative assimilation trajectories for mafic granulites lying along the terrestrial array exhibited a poorer fit and, for simplicity, are not shown. We assume that the intermediate granulite has comparatively enriched (unradiogenic) Hf and Nd isotopes and resembles intermediate-SiO_2 granulite xenoliths from South Africa and measured by Schmitz et al. (2004) (Table S1). Several Pb isotopic compositions were tested for the LCC assimilation scenarios to determine the best fit to the measured ENA CAMP data set (see Figure 3, Table S1, S2), considering the large span of Pb isotopic ratios exhibited by the basement terranes previously accreted to ENA (Pettingill et al., 1984; Sinha et al., 1996; Whalen et al., 2015). Because well-characterized intermediate-SiO_2 granulite xenoliths in the literature are largely peraluminous, a composition that may not be representative of all lower crust, we further tested a more aluminum-poor composition based on well-characterized, intermediate-SiO_2 granulites from Jonsa, Finland (Nehring et al., 2010); however, the Finnish granulite composition likewise exhibited a poorer fit than the other results, so for simplicity it is not shown.

We show our calculated crustal assimilation trajectories in Figure 3. Only the relatively enriched, intermediate-SiO_2 granulite assimilant can account for most of the Hf-Nd isotopic variability observed in our samples with 10% assimilation or less (Figure 3). Up to 10% assimilation of Carolina terrane UCC rocks cannot explain most of the ε_{Hf}-ε_{Nd} data array (Figure 3). Mafic LCC assimilation trajectories deviate to much higher ε_{Hf} than our sample data (Figure 3) when using the isotopically decoupled assimilant after Zartman et al. (2013), and none of the mafic granulite

Pb isotope compositions tested are able to explain our samples' Pb isotopes using only 10% addition (see also Callegaro et al., 2013; Merle et al., 2014; Whalen et al., 2015). For intermediate-SiO_2 LCC, the Pb isotope composition of an assimilant needs to be relatively unradiogenic (e.g., $^{206}Pb/^{204}Pb$ ~17.0-17.3), but the assimilant must also have relatively unradiogenic $^{176}Hf/^{177}Hf$ and $^{143}Nd/^{144}Nd$ compositions (Figure 3). Such a low $^{206}Pb/^{204}Pb$ composition may be plausible when compared with the ranges measured in granulites from Antarctica (Wysoczanski et al., 1995), Scotland (Halliday et al., 1993), and Michigan (Zartman et al., 2013), which provide global examples of intermediate to felsic lower crustal granulites, and also in light of the low $^{206}Pb/^{204}Pb$ signatures observed in some exposed Carolina terrane rocks (granulites, charnockites, and anorthosites; Sinha et al., 1996).

All of our LCC assimilation calculations exhibit concave-down curvature in Figure 3, suggesting that, e.g., Pb may generally be more significantly impacted than Hf by assimilation processes because of its higher concentrations in granulitic basement relative to mantle-derived basalts (e.g., Zartman et al., 2013). We further note that among our tested compositions, only a crustal contaminant containing accessory zircon, like our intermediate-SiO_2 granulite composition, had sufficiently high Hf partition coefficients to reproduce the isotope compositions observed in our southern ENA data set with only 10% assimilation. In our calculations, the presence of minor zircon in the assimilant rock also extends the compositions of magmas experiencing even minor assimilation to more highly unradiogenic ε_{Hf} values (Figure 3). The role of accessory minerals in magma assimilation processes is, however, presently unclear and likely to be more complex than our models allow. For example, minerals like zircon may be effectively dissolved from country rocks adjacent to mafic sills and dikes early in the melt-rock interaction process, depending on local zircon abundance, grain size, and Zr saturation in the melt (e.g., Bindeman & Melnik,

2016). Melt-rock interaction between intruding magmas and granulitic country rocks is also likely to be highly variable both spatially and over time, beyond the relatively simple calculated scenarios shown in Figure 3. We thus only conclude that limited absorption of intermediate-SiO_2, relatively isotopically enriched granulitic wallrock by primary CAMP tholeiitic magmas may in part account for elevation of southern ENA samples above the terrestrial data array, within the 10% assimilation constraint previously identified using Os isotopes (Callegaro et al., 2013; Merle et al., 2014).

4.2. Source origins of Eastern North American tholeiites

While assimilation of crust may play a role in generating part of the isotopic variability observed, some observations, such as the complex Pb isotope systematics, still favor additional mantle source heterogeneity effects to fully explain the origins of ENA CAMP (Callegaro et al., 2013; Merle et al., 2014; Whalen et al., 2015). Based on their distribution, much of the isotopic variations observed in ENA CAMP tholeiite samples may require the involvement of multiple distinct mantle sources (Figure 2). Below we explore current working hypotheses for heterogeneous source origins of the southern ENA CAMP data set, including 1) global mantle reservoirs, 2) SCLM, and 3) recently recycled crust in the local asthenosphere.

4.2.1. Hypothesis 1: Global mantle reservoirs as a source for CAMP

A technique for identifying possible plume-derived and/or long-lived mantle reservoirs for the central Atlantic region is considering the end member basalt compositions observed in local ocean island basalts, such as the Azores (Béguelin et al., 2017), Madeira (Geldmacher et al., 2011), or Bermuda (Mazza et al., 2019), as well as Mesozoic MORB (Janney & Castillo, 2001) and recently identified Eocene magmatism in the Appalachians (Mazza et al., 2017) (Figure 2).

However, prior research (e.g., Marzoli et al., 2019, and references therein) has consistently shown that such end-members cannot explain all of the isotopic compositions observed in CAMP, and indeed Atlantic intraplate basalts span a notably different compositional range than that observed across the ENA CAMP data set.

Long-lived mantle components, such as depleted MORB mantle (DMM) and the most extreme enriched mantle end-members (EM-1 and EM-2), define a broader range of isotopic compositions, and their potential contribution in generating the observed trends in CAMP compositions is examined here. This scenario resembles the proposed origin for many hotspot volcanic centers and ocean islands, and would potentially suggest the presence in the melt zone of materials transported from the deep mantle via a mantle plume. However, recent isotope measurements of ENA CAMP have demonstrated that mixing of long-lived, global mantle components in a heterogeneous mantle source is unable to fully explain the range of isotope compositions observed, particularly for Pb isotope ratios (Callegaro et al., 2013, 2014, 2017; Merle et al., 2011, 2014), and that outcome remains unchanged by our new Hf contributions as demonstrated by our mixing calculations (Figures 4, 5). In those calculations, we test more recent estimates for the isotopic compositions of EM-1 and EM-2 (e.g., Jackson and Dasgupta, 2008; Jackson et al., 2007; Table S1), which have less extreme Pb isotope compositions than, e.g., earlier estimates that were used in prior CAMP studies (e.g., Whalen et al., 2015); our results do not, however, achieve a better fit to ENA CAMP isotopic data than previous work. We further note that while parts of our data set resemble partial melts of enriched mantle reservoirs like EM-1 or EM-2, the trend of the southern ENA CAMP data array is inconsistent with the sense of enrichment implied by mixing trajectories in Figures 4 and 5. In particular, the samples with isotopic signatures towards the low-ε_{Hf} end of the data array (i.e., trending towards enriched

mantle) also exhibit relatively low Pb isotope ratios and thus appear to trend away from the same end members in Pb-isotope space. This apparent mismatch indicates that additional partial melt sources must be considered to fully explain the origins of southern ENA CAMP.

4.2.2. Hypothesis 2: Melting of subcontinental lithospheric mantle

It is possible that the lithospheric mantle beneath CAMP has experienced prior melting (e.g., during rifting of Laurussia) that may have left a depleted and refractory lithospheric mantle residue. The moderately high temperatures calculated for CAMP (Herzberg & Gazel, 2009) may have then been sufficient to cause melting of the refractory SCLM: at temperatures of 1480ºC and relatively low mantle pressures (1.5-2.0 GPa), Falloon and Danyushevsky (2000) predicted 6-12% melting of anhydrous harzburgite. This refractory mantle should be depleted in incompatible trace elements and thus may resemble depleted asthenospheric mantle in trace element and isotopic composition, making it difficult to uniquely identify. We note that in this scenario, heating and melting of refractory lithosphere would need to be sufficiently widespread to explain the large volume of magma likely deposited during CAMP. The total volume emplaced remains unknown, but the province spans a total area of approximately 10^7 km^2, as noted above. We further note that mantle temperatures sufficient to remelt refractory SCLM are also sufficient to melt the more fertile underlying lherzolitic asthenosphere, and the geochemical signatures of these two scenarios are expected to significantly overlap. Such asthenospheric melting is likely to produce an additional volume of magma that would overwhelm the trace element contribution from the less fertile, trace element depleted, harzburgitic lithospheric rocks.

On the other hand, supra-subduction zone SCLM, such as that produced during the assembly of Pangea, is further expected to be variably infiltrated by metasomatic fluids that would impart a

more enriched trace element and isotopic composition. A metasomatized SCLM is thus an alternative and more fertile melt source that has been suggested for CAMP tholeiites (e.g., Alibert, 1985; Bertrand, 1991; Bertrand et al., 1982; Cebriá et al., 2003; De Min et al., 2003; Deckart et al., 2005; Dostal & Durning, 1998; Dupuy et al., 1988; Heatherington & Mueller, 1999; Jourdan et al., 2003; Marsh, 1987; Merle et al., 2011; Pegram, 1990; Puffer, 1992; Puffer, 2003), including high-TiO_2 CAMP magmas from Sierra Leone (Callegaro et al., 2017). In Sierra Leone, high-TiO_2 gabbros of the Freetown Layered Complex exhibit an enriched isotopic signature characterized by very high $^{207}Pb/^{204}Pb_{201Ma}$ ratios but low $^{206}Pb/^{204}Pb_{201Ma}$ (Figure 2). A small amount of lamproite magma, inferred to derive from a local, subduction-metasomatized SCLM source, was tested as a plausible contributor, mixed with a dominant asthenospheric melt (Callegaro et al., 2017). A group of high-TiO_2 samples from South America (Merle et al., 2011) with comparatively low $^{207}Pb/^{206}Pb$ (Figure 2) may also sample a distinct, localized mantle or SCLM source (Merle et al., 2011). While a portion of the field for southern ENA CAMP Pb isotope signatures overlaps with that of Sierra Leone gabbros (Figure 2), they are otherwise distinct, having low TiO_2 contents, higher $^{87}Sr/^{86}Sr_{201Ma}$, and lower $^{143}Nd/^{144}Nd_{201Ma}$ than the Freetown gabbros.

Without local volcanic samples inferred to derive from SCLM melt sources, or SCLM-derived local xenoliths for comparison, there are no regional Hf isotopic constraints for southern ENA SCLM, making it difficult to directly test for SCLM melt contributions to southern ENA CAMP basalts. Eastern North American CAMP was located farther from cratonic or peri-cratonic settings than magmas from Brazil or Sierra Leone, though, suggesting SCLM is a less likely melt source for ENA. We further note that although there are rare exceptions (e.g., Griffin et al., 2000), global SCLM xenolith data largely have $\varepsilon_{Hf} > +9$ (Choi et al., 2008, 2010; Shaw et al.,

2007; Wittig et al., 2007, 2010) (Figure S2), making it difficult to explain the observed array primarily by this mechanism. We cannot completely rule out an exotic, metasomatized lithospheric mantle melt component influencing the composition of individual samples with slightly elevated ε_{Hf} (Figure 2a), but based on prior work, we consider it an unlikely overall melt source for low-TiO_2 LIP tholeiites.

4.2.3. Hypothesis 3: Paleozoic crustal recycling in the asthenosphere beneath CAMP

In a third scenario, we explore Paleozoic recycling of crustal material and production of a modified mantle source beneath ENA, which is subsequently melted during the CAMP event. Callegaro et al. (2013) suggested that ENA magmas may derive from direct melting of local asthenosphere containing 1) depleted upper mantle, 2) recycled upper continental crustal rocks, possibly as subducted Paleozoic terrigenous sediments associated with the assembly of Pangea, and 3) lower continental crustal rocks, perhaps delaminated and locally reintroduced into the convecting melt region (see e.g., Magni and Király, 2019). Whalen et al. (2015) suggested a related scenario in which melts and/or aqueous fluids derived from subducted sediments modified the local mantle melt source beneath ENA, with a stronger fluid-derived signature in the south and more melt metasomatism recorded to the north. Below, we explore the constraints that Hf isotopes would place on both models, and attempt to evaluate the possible role of Paleozoic recycled crust in ENA CAMP magma generation.

4.2.3.1. Paleozoic recycling of upper and lower continental crust. Crustal recycling provides possible explanations for an incompatible-element enriched source with notably high Lu/Hf ratios, as implied by the radiogenic $\varepsilon_{Hf\ 201Ma}$ relative to $\varepsilon_{Nd\ 201Ma}$ observed in southern ENA CAMP. As an initial test of melting a subduction-modified mantle source, we first consider

460 whether direct mixing of local depleted asthenospheric mantle melts with recycled upper and
461 local crust, i.e. the scenario suggested by Callegaro et al. (2013), can directly produce the
462 observed data array (Figure 6). As discussed above, most continental crustal rocks plot along the
463 terrestrial array, making it difficult to reproduce the southern ENA data trend. However, some
464 lower crustal mafic granulites may inherit a high, decoupled ε_{Hf} ratio due to the presence of
465 significantly old garnet with high Lu/Hf ratios (e.g., Blichert-Toft et al., 2005), similar to some
466 of the xenoliths measured by Zartman et al. (2013). If recycled, e.g., by delamination into the
467 asthenosphere, mafic LCC thus represents a plausible mantle source with elevated ε_{Hf} above the
468 mantle array in Figure 2a. However, an additional unradiogenic (enriched) Hf source lying closer
469 to the mantle array would then also be required to fully explain the observed ENA data. Upper
470 continental crust is typically more enriched in incompatible elements and should plot along the
471 mantle array (Table S1, Figures 2a, 4), making it a reasonable, additional recycled source and
472 possibly lending support to the suggested model of Callegaro et al. (2013). Upper crustal
473 material could have been introduced to the regional mantle by subduction of terrigenous marine
474 sediments; if local sediment deposition occurred near a subducting margin and was relatively
475 close to a weathering continental source, such sediments would closely resemble the average
476 composition of nearby continental terranes, as modeled by Callegaro et al. (2013).

477 However, we observe that direct mixing of melts from ambient asthenosphere with a typical DM
478 isotopic composition (Salters and Stracke, 2004; Workman and Hart, 2005) with recycled LCC
479 and UCC material is unable to explain the Hf and Pb isotopes measured for southern ENA
480 CAMP, at least within currently available constraints (e.g., Figure 2b). This is illustrated by the
481 isotopic compositions of the suggested end-members in Table S1 and Figure 2b, where we
482 identify a Proterozoic lower crustal end-member represented by mafic granulite Michigan

483 xenoliths ("Mafic LCC," Zartman et al., 2013), an upper crust end-member represented by local
484 average Carolina terrane ("UCC") ($^{206}Pb/^{204}Pb$ ranges between ca. 17.1 and 17.5 for Carolina
485 terrane rocks; Pettingill et al., 1984; Sinha et al., 1996), and ambient mantle modeled as a DM
486 component ("DMM"). In particular, crustal components with ε_{Hf} and ε_{Nd} values capable of
487 explaining the CAMP array do not span a sufficiently large range in Pb isotopic compositions to
488 explain the measured data (Figure 2).

489 *4.2.3.2. Paleozoic recycling and metasomatism of the asthenosphere.* Alternatively, Whalen et al.
490 (2015) suggested a scenario for the recycling of regional Paleozoic upper crustal sediments into
491 the subcontinental asthenosphere without invoking lower crustal delamination. By incorporating
492 subducted pelagic marine sediments, this scenario offers an alternative to recycled local UCC
493 from the Carolina terrane, one that notably plots above the mantle array; such a component may
494 thus alleviate the need for melting of exotic (i.e., with decoupled ε_{Hf} and ε_{Nd}) mafic Proterozoic
495 LCC rocks. Unlike our upper crust estimate for the Carolina terrane, weathered terrigenous
496 marine sediments have elevated Lu/Hf ratios due to the progressive removal of heavy detritus
497 minerals like zircon during continental weathering and differential river transport; the elevated
498 Lu/Hf ultimately produces high ε_{Hf} relative to ε_{Nd} in clay-rich marine pelagic sediments (Chauvel
499 et al., 2014; Garcon et al., 2013, 2014; Vervoort et al., 1999, 2011). Chauvel et al. (2008)
500 determined time-averaged ε_{Hf} and ε_{Nd} isotope compositions for typical subducted sediments,
501 which reside in the same part of the Hf-Nd isotope diagram as both marine Fe-Mn precipitates
502 and seawater (e.g., Albarede et al., 1998) (Figure 2a). As an alternative to the prior mixing
503 scenario with upper and lower continental crust, here we test mixing of partial melts of depleted
504 asthenosphere with a combination of 1) local Carolina terrane crust and 2) global average marine
505 sediments (GLOSS, after Plank and Langmuir (1998) and Chauvel et al. (2008); Table S1).

Specifically, we tested a Paleozoic marine sediment source subducted beneath the CAMP province during the construction of Pangea at ~370 Ma, i.e., 170 Ma prior to the CAMP melting event, after Merle et al. (2014), Callegaro et al. (2013), and Whalen et al. (2015).

In Figure 6a, where mixing results are reported along with our data, ternary mixing of depleted mantle, Carolina UCC crust, and average global sediment cannot account for the Hf-Nd isotopic variability observed in ENA samples. While trace element concentrations in recycled sources are necessarily averages of heterogeneous materials, and a small change in the trace element budget of upper crust, for example, may appear to resolve the observed discrepancy in mixing trajectories, the end members are inconsistent between diagrams. That is, average global subducted sediment has elevated ε_{Hf} relative to ε_{Nd}, similar to the southern ENA data array (e.g., Chauvel et al., 2008; Chen et al., 2013; Vervoort et al., 2011), but its highly radiogenic Pb isotope ratios are inconsistent with our most extreme samples, which have the lowest $\varepsilon_{Nd\ 201Ma}$ but also the least radiogenic $^{206}Pb/^{204}Pb_{201Ma}$ and $^{207}Pb/^{204}Pb_{201Ma}$. While contributions of melts from recycled crustal rocks could thus explain some of the intermediate compositions observed in the ENA CAMP data set, the scenario is a poor explanation for the most unradiogenic samples with respect to $\varepsilon_{Hf\ 201Ma}$.

A more plausible recycling hypothesis is the creation of a hybrid, metasomatised mantle source by the addition of subduction-derived fluids to the peridotitic mantle wedge, which in turn partially melts to produce local CAMP tholeiites. Whalen et al. (2015) suggested that the subducted sediments in the subcontinental CAMP asthenosphere have dehydrated and/or melted, producing fluids that metasomatically modified ambient peridotite. They further tied the nature

527 of the metasomatic fluid (aqueous fluid in the south vs. silicate melt in the north) to geographic
528 variations along the ENA subprovince as noted above.

529 Hafnium is primarily considered a tracer of melt and not aqueous fluid metasomatism in modern
530 arc environments (e.g., Kempton et al., 2018), because Hf is expected to have relatively low
531 aqueous solubility (e.g., Banks, 1950; Linnen, 1998). However, the relatively low fluid mobility
532 of Hf means dehydration of subducted sediments may produce a relatively high Lu/Hf
533 metasomatic fluid, such that a modified mantle may develop relatively high ε_{Hf} ratios over time
534 (e.g., Janney et al., 2005; Kempton et al., 2018). If northern ENA tholeiites record primarily melt
535 metasomatism while southern ENA tholeiites record ancient fluid metasomatism of the regional
536 mantle source, as posited by Whalen et al. (2015), southern ENA mantle could then have
537 developed variably high ε_{Hf} compared to ε_{Nd}, while northern ENA mantle did not, similar to our
538 observations; however, such a difference in fluid vs. melt metasomatic effects could be
539 confounded by other factors. For instance, subducted metasediments may include stable
540 metamorphic garnet, which could impact the Lu/Hf ratio of metasomatizing melts or fluids
541 derived from the subducted rocks (e.g., Kempton et al., 2018). Some lithospheric mantle
542 xenoliths that have experienced metasomatism also have extremely high ε_{Hf} ratios, unlike ENA
543 CAMP basalts (e.g., Armytage et al., 2015). The impact of metasomatic source effects on long-
544 term $^{176}Hf/^{177}Hf$ ratios is thus unclear and warrants more careful analysis.

545 Here we introduce a new model for calculating the trace element and isotope compositions of
546 both subduction-modified depleted mantle wedge and subsequent partial melts of that modified
547 mantle source (Table S4). In the model, three initial reservoirs are age-corrected to the time of
548 subduction recycling: 1) ambient peridotite asthenosphere after Salters and Stracke's (2004)

549 Depleted Mantle; 2) average global oceanic sediment similar to GLOSS (Chauvel et al., 2008;
550 Plank and Langmuir, 1998); and 3) altered oceanic crust (AOC) calculated from Atlantic drill
551 core compositions (Staudigel et al., 1996). The composition of a metasomatizing fluid is then
552 determined for a range of mixtures of 1) an AOC-derived aqueous fluid and 2) either a melt or an
553 aqueous fluid derived from subducted sediment. Trace element concentrations in all AOC and
554 sediment-derived fluids are calculated using mobility and partition coefficients after Kogiso et al.
555 (1997), Stracke et al. (2003), and Johnson and Plank (2000) (Table S3; see Supporting
556 Information). The composition of the modified wedge is then determined for 0-10% fluid
557 addition to the mantle, and across the full range of fluid mixtures. Next, the resulting modified
558 mantle composition is tracked for isotopic decay from the time of recycling and metasomatism
559 (370 Ma) until the time of melting (201 Ma) to determine the isotopic and trace element
560 compositions of the mantle during CAMP. Predicted trace element compositions in CAMP
561 basalts were determined using a simple modal batch melting model and melt fraction of 6%, with
562 garnet lherzolite mineral/melt partition coefficients and residual peridotite modes as in Table S3.

563 Results from the wedge metasomatism and melting model, shown in Figure 7, approach or
564 overlap with the most isotopically depleted southern ENA CAMP basalt composition (sample
565 CS49), as long as the subduction and recycling age is relatively young. The results shown in
566 Figure 7 assume a Paleozoic subduction age of 370 Ma, i.e. the recycling age previously
567 suggested by Merle et al. (2014), Callegaro et al. (2013), and Whalen et al. (2015). Recycling
568 ages older than Paleozoic subduction fail to reproduce the $\varepsilon_{Hf\ 201Ma}$, $\varepsilon_{Nd\ 201Ma}$, and Pb isotope
569 ratios observed in our basalts. Melting of a mantle source modified by a purely aqueous
570 metasomatic fluid and dominated by sediment-derived fluid (i.e., the AOC-derived fluid $\leq$ 25%
571 of the fluid mixture) can reasonably explain sample CS49 with less than 10% fluid addition,

572 although we note that the Pb isotope results shown in Figure 7c are close but not an exact fit to
573 the measured data at the lowest fluid addition values (< 4%) that work best for ε_{Hf} and ε_{Nd}
574 isotopes.

575 We further note that for the most radiogenic Pb isotopes observed in ENA CAMP tholeiites,
576 mantle metasomatism dominated by aqueous fluid addition is a closer match than melt
577 metasomatism, even for some Newark basin samples (Figure 7c). This observation conflicts with
578 the suggestion of Whalen et al. (2015) that differences in Paleozoic subduction angles modified
579 the metasomatic regime from north to south beneath the North American margin, and that more
580 northerly ENA tholeiites were dominated by melt- and not aqueous fluid metasomatism of the
581 Paleozoic mantle. We would argue that while the exact proportions of fluid addition to the
582 mantle wedge may have been variable, a fluid-dominated metasomatic agent where most of the
583 fluid is derived from subducted sediments (i.e., only a limited proportion of the fluid is
584 contributed by AOC) provides a particularly good match to the radiogenic $^{206}Pb/^{204}Pb$ ENA end-
585 member (Figure 7).

586 *4.2.3.3. A hybrid recycling, metasomatism, and assimilation model for ENA CAMP.*

587 While the most primitive ENA CAMP magma analyzed here is in good agreement with
588 predictions for melting of metasomatized mantle, the remainder of our observed data array
589 cannot be explained purely by melting of such a source, even if the nature of that metasomatism
590 is itself regionally variable. Additional melting, mixing, and/or assimilation is thus required to
591 explain the full isotopic range exhibited by southern ENA CAMP. As explored above, the
592 compositions of southern ENA samples with low $\varepsilon_{Nd\ 201Ma}$, comparatively radiogenic $\varepsilon_{Hf\ 201Ma}$,
593 and relatively low $^{206}Pb/^{204}Pb_{201Ma}$ cannot be easily explained by melt mixing. Of the possible

sources considered here, only lower crustal granulites with decoupled Lu/Hf and Sm/Nd have the necessary isotopic signatures to plausibly explain this composition, but the required proportional contributions of melts from such a source are inconsistent in our calculations (Figure 8), and are too large for some of the resulting mixtures to be basaltic in major element composition. Based on the analysis above, we thus suggest that the ENA CAMP mantle melt source is dominated by fluid-metasomatized asthenosphere, perhaps containing moderate quantities of recycled continental crustal material, but not so much all of the observed data can be explained by direct melting of those recycled rocks. Some minor (generally < 10%) assimilation of zircon-bearing, intermediate-SiO_2, granulitic lower crust can then help to explain much of the southern ENA data array (Figure 3). Our favored model thus includes a combination of factors, where some direct melting of recycled crust is plausible, but minor crustal assimilation is also favored, particularly to explain the southern ENA CAMP samples with the lowest $\varepsilon_{Hf\ 201Ma}$ values. We consider this a plausible model to explain the systematic trend towards low $\varepsilon_{Nd\ 201Ma}$ and $^{206}Pb/^{204}Pb_{201Ma}$ with comparatively high $\varepsilon_{Hf\ 201Ma}$ and $^{207}Pb/^{204}Pb_{201Ma}$ in southern ENA basalts.

4.3. Broader petrogenesis of Central Atlantic Magmatic Province tholeiites

Figure 2a includes $^{176}Hf/^{177}Hf_{201Ma}$ results for magmas collected from other regions of CAMP, including Sierra Leone and Morocco (Table 2). The range of isotopic compositions across CAMP reflects localized processes, which for ENA include a local metasomatized mantle source and minor assimilation of local crustal rocks. Such localized variations extend to other parts of CAMP as well: samples from Sierra Leone, as noted above, exhibit notably high $\varepsilon_{Hf\ 201Ma}$ values for a given $^{206}Pb/^{204}Pb_{201Ma}$ ratio (Figure 2b) and have been suggested to incorporate melts from local SCLM sources unique to that region, with an enriched composition comparable to

worldwide anorogenic lamproites, e.g. from Western Australia, Gaussberg, or Leucite Hills (Callegaro et al., 2017). Likewise, in Pb isotope space, most magmas from CAMP form an array with high $^{207}Pb/^{204}Pb_{201Ma}$ for a given $^{206}Pb/^{204}Pb_{201Ma}$, while high-$TiO_2$ samples from South America have comparatively lower $^{207}Pb/^{204}Pb_{201Ma}$ for a given $^{206}Pb/^{204}Pb_{201Ma}$ (Figure 2) (Merle et al., 2011) and may instead sample a localized mantle or SCLM source, as noted above (Deckart et al., 2005; Merle et al., 2011). Central Atlantic Magmatic Province rocks from Guyana, Brazil, and Sierra Leone also include high-TiO_2 tholeiites (TiO_2 > 2 wt. %). The high-TiO_2 CAMP magma type, which exhibits very distinct isotopic signatures and trace element compositions (Marzoli et al., 2018), is volumetrically minor and confined to a narrow belt bordering the Western African Craton and the Amazonia Craton/Guyana Shield (De Min et al., 2003; Deckart et al., 2005; Dupuy et al., 1988; Mauche et al., 1989).

The above observations indicate that a number of isotopic patterns are unique to specific regions within CAMP and sample localized sources in the underlying mantle. The more geographically restricted patterns do not clearly indicate a radially distributed hotspot-like signature that might directly support mantle plume influence. Even if the arrival of a plume head was associated with more widespread geographic dispersal and magma emplacement across broader terranes (e.g., McHone, 1996), making geographic emplacement patterns far from radial, such episodes should follow a sequence where first SCLM is melted due to thermal erosion, and then upwelling asthenospheric mantle melts (e.g., Ernst & Buchan, 2003; Ernst et al., 2001; Morgan, 1983). Based on isotope measurements and age information, neither scenario (geographically radial distribution of isotopic enrichment, or timing sequences indicative of large-scale lithospheric erosion and melting followed by asthenospheric melting) appears clear for CAMP.

Instead, the more localized geographic patterns appear to support regional upwelling and melting of local mantle, including localized melting of SCLM for some areas. Our observations could thus plausibly be explained either 1) by a regional passive upwelling response to lithospheric thinning, i.e., localized mantle convection response to rift initiation, or 2) by the arrival of a deep upwelling mantle plume and accompanying melting of entrained local asthenosphere and, in some areas, overlying lithosphere. A province-wide geochemical plume signature for CAMP thus remains ambiguous.

5. CONCLUSIONS

Eastern North American CAMP basalts were plausibly generated by melting of regionally upwelling, depleted upper mantle asthenosphere, which was likely metasomatized by aqueous fluids derived from subducted oceanic crust and marine sediments. That melting may have been accompanied by direct melting of relatively minor quantities of previously recycled (e.g., subducted or delaminated) crustal rocks. Melting was likely then followed by assimilation of lower continental crust, possibly intermediate-SiO_2 granulites containing minor accessory minerals like zircon, which may influence the hafnium isotopic compositions of the basalts. The isotopic compositions of CAMP basalts do not directly support dominantly OIB-like, long-lived, enriched mantle source reservoir origins, but instead vary with local upper mantle and lithospheric compositions across the province, recording broad, regional mantle upwelling. Our findings thus suggest that continental rifting and the generation and emplacement of the CAMP flood basalt province are best explained by regional asthenospheric decompression beneath the Pangea supercontinent, neither requiring nor definitively precluding the influence of a deep-seated mantle plume on continental rifting.

Acknowledgments

We thank Jörg Geldmacher, Pamela Kempton, and two anonymous reviewers for providing thoughtful suggestions that helped improve a prior version of this manuscript. We also thank John Lassiter and Steve Shirey for productive discussions about CAMP. Daren Blythe and Nathan Sorsen assisted with sample preparation at UNL. L. Elkins acknowledges support from a UNL College of Arts and Sciences International Collaboration Award that funded this research. Field sampling was supported by the following grants: CARIPARO (Eccellenza 2008), PRIN (PRIN 20158A9CBM), Padova University (CPDA132295/13) to A. M. N. Youbi (Caddi Ayyad University, Marrakech, Morocco), H. Bertrand (ENS-Lyon, France), G. Bellieni (Padova University, Italy), S. Howard (South Carolina Survey), and M. Higgins (North Carolina Survey) are kindly thanked for help during fieldwork. Supporting data files are available at the IEDA data repository (https://doi.org/10.1594/IEDA/111347).

REFERENCES

Albarede, F., A. Simonetti, J. D. Vervoort, J. Blichert-Toft, and W. Abouchami (1998), A Hf-Nd isotopic correlation in ferromanganese nodules, *Geophysical Research Letters*, *25*(20), 3895-3898.

Alibert, C. (1985), A Sr-Nd isotope and REE study of late Triassic dolerites from the Pyrenees (France) and the Messejana Dyke (Spain and Portugal), *Earth and Planetary Science Letters*, *73*(1), 81-90.

679 Anderson, D. L. (1994), The sublithospheric mantle as the source of continental flood basalts:
680 The case against the continental lithospher and plume head reservoirs, *Earth and Planetary*
681 *Science Letters*, *123*, 269-280.

682 Armytage, R. M., A. D. Brandon, R. Andreasen, and T. J. Lapen (2015), Evolution of Mojavian
683 mantle lithosphere influenced by Farallon plate subduction: Evidence from Hf and Nd isotopes
684 in peridotite xenoliths from Dish Hill, CA, *Geochimica et Cosmochimica Acta*, *159*, 264-284.

685 Baksi, A. K. (2003), Critical evaluation of $^{40}Ar/^{39}Ar$ ages for the Central Atlantic Magmatic
686 Province: timing, duration and possible migration of magmatic centers, *Geophysical Monograph*
687 *Series*, *136*, 77-90.

688 Banks, H. O. (1950), The determination of the solubility of hafnium oxide in aqueous solution by
689 the radioactive tracer technique, 4822 pp, School of Mines and Metallurgy of the University of
690 Missouri, Rolla, Missouri.

691 Bédard, J. (1992), Jurassic quartz-normative tholeiite dikes from Anticosti Island, Quebec, In
692 *Eastern North American Mesozoic Magmatism*, Eds. Puffer, J.H. and P.C. Ragland, *Special*
693 *Papers-Geological Society of America*, v. 268, 161.

694 Begemann, F., K. Ludwig, G. Lugmair, K. Min, L. Nyquist, P. Patchett, P. Renne, C.-Y. Shih, I.
695 M. Villa, and R. Walker (2001), Call for an improved set of decay constants for
696 geochronological use, *Geochimica et Cosmochimica Acta*, *65*(1), 111-121.

697 Béguelin, P., M. Bizimis, C. Beier, and S. Turner (2017), Rift–plume interaction reveals multiple
698 generations of recycled oceanic crust in Azores lavas, *Geochimica et Cosmochimica Acta*, *218*,
699 132-152.

Bertrand, H. (1991), *The Mesozoic tholeiitic province of Northwest Africa; a volcanotectonic record of the early opening of Central Atlantic*, In *Magmatism in extensional structural settings: the Phanerozoic African Plate*, Eds. Kampunzu, A.B. and R.T. Lubala, Springer-Verlag, Berlin, Germany.

Bertrand, H., J. Dostal, and C. Dupuy (1982), Geochemistry of early Mesozoic tholeiites from Morocco, *Earth and Planetary Science Letters*, *58*(2), 225-239.

Bindeman, I. N., and O. E. Melnik (2016), Zircon survival, rebirth and recycling during crustal melting, magma crystallization, and mixing based on numerical modelling, *Journal of Petrology*, *57*(3), 437-460.

Blackburn, T. J., P. E. Olsen, S. A. Bowring, N. M. McLean, D. V. Kent, J. Puffer, G. McHone, E. T. Rasbury, and M. Et-Touhami (2013), Zircon U-Pb geochronology links the end-Triassic extinction with the Central Atlantic Magmatic Province, *Science*, *340*(6135), 941-945.

Blichert-Toft, J. (2001), On the Lu-Hf isotope geochemistry of silicate rocks, *Geostandards Newsletter-the Journal of Geostandards and Geoanalysis*, *25*(1), 41-56.

Blichert-Toft, J., F. A. Frey, and F. Albarede (1999), Hf isotope evidence for pelagic sediments in the source of Hawaiian basalts, *Science*, *285*(5429), 879-882.

Blichert-Toft, J., A. Agranier, M. Andres, R. Kingsley, J. G. Schilling, and F. Albarede (2005), Geochemical segmentation of the Mid-Atlantic Ridge north of Iceland and ridge-hot spot interaction in the North Atlantic, *Geochemistry Geophysics Geosystems*, *6*, 10.1029/2004GC000788.

720 Bohrson, W. A., and F. J. Spera (2001), Energy-constrained open-system magmatic processes II:
721 application of energy-constrained assimilation–fractional crystallization (EC-AFC) model to
722 magmatic systems, *Journal of Petrology*, *42*(5), 1019-1041.

723 Bouvier, A., J. D. Vervoort, and P. J. Patchett (2008), The Lu–Hf and Sm–Nd isotopic
724 composition of CHUR: constraints from unequilibrated chondrites and implications for the bulk
725 composition of terrestrial planets, *Earth and Planetary Science Letters*, *273*(1-2), 48-57.

726 Bryan, S. E., and R. E. Ernst (2008), Revised definition of large igneous provinces (LIPs), *Earth-*
727 *Science Reviews*, *86*(1-4), 175-202.

728 Burov, E., and T. Gerya (2014), Asymmetric three-dimensional topography over mantle plumes,
729 *Nature*, *513*(7516), 85.

730 Callegaro, S., A. Marzoli, H. Bertrand, M. Chiaradia, L. Reisberg, C. Meyzen, G. Bellieni, R. E.
731 Weems, and R. Merle (2013), Upper and lower crust recycling in the source of CAMP basaltic
732 dykes from southeastern North America, *Earth and Planetary Science Letters*, *376*, 186-199.

733 Callegaro, S., D.R. Baker, A. De Min, A. Marzoli, K. Geraki, H. Bertrand, C. Viti, and F.
734 Nestola (2014), Enriched mantle source for the Central Atlantic magmatic province: New
735 supporting evidence from southwestern Europe, *Lithos*, *188*, 15-32.

736 Callegaro, S., A. Marzoli, H. Bertrand, J. Blichert-Toft, L. Reisberg, G. Cavazzini, F. Jourdan,
737 J.H. Davies, L. Parisio, R. Bouchet, A. Paul, U. Schaltegger, M. Chiaradia (2017), Geochemical
738 Constraints Provided by the Freetown Layered Complex (Sierra Leone) on the Origin of High-Ti
739 Tholeiitic CAMP Magmas, *Journal of Petrology*, *58*(9), 1811-1840.

740 Capriolo, M., A. Marzoli, L.E. Aradi, S. Callegaro, J. Dal Corso, R.J. Newton, B.J.W. Mills, P.B.
741 Wignall, O. Bartoli, D.R. Baker, N. Youbi, L. Remusat, R. Spiess, and C. Szabó, (2020), Deep
742 CO_2 in the end-Triassic Central Atlantic Magmatic Province, *Nature Communications 11*, 1670,
743 doi: 10.1038/s41467-020-15325-6.

744 Carlson, R. (1991), Physical and chemical evidence on the cause and source characteristics of
745 flood basalt volcanism, *Australian Journal of Earth Sciences*, *38*(5), 525-544.

746 Cebriá, J. M., J. López-Ruiz, M. Doblas, L. T. Martins, and J. Munha (2003), Geochemistry of
747 the Early Jurassic Messejana-Plasencia dyke (Portugal-Spain); Implications on the Origin of the
748 Central Atlantic Magmatic Province, *Journal of Petrology*, *44*, 547-568.

749 Chabou, M. C., H. Bertrand, and A. Sebaï (2010), Geochemistry of the Central Atlantic
750 Magmatic Province (CAMP) in south-western Algeria, *Journal of African Earth Sciences*, *58*,
751 211-219.

752 Chauvel, C., E. Lewin, M. Carpentier, N. T. Arndt, and J. C. Marini (2008), Role of recycled
753 oceanic basalt and sediment in generating the Hf-Nd mantle array, *Nature Geoscience*, *1*(1), 64-
754 67.

755 Chauvel, C., E. Lewin, M. Carpentier, N. T. Arndt, and J.-C. Marini (2008), Role of recycled
756 oceanic basalt and sediment in generating the Hf–Nd mantle array, *Nature geoscience*, *1*(1), 64.

757 Chauvel, C., M. Garcon, S. Bureau, A. Besnault, B. M. Jahn, and Z. L. Ding (2014), Constraints
758 from loess on the Hf-Nd isotopic composition of the upper continental crust, *Earth and*
759 *Planetary Science Letters*, *388*, 48-58.

760 Chen, T.-Y., G. Li, M. Frank, H.-F. Ling (2013), Hafnium isotope fractionation during
761 continental weathering: Implications for the generation of the seawater Nd-Hf isotope
762 relationships, *Geophysical Research Letters*, *40*, 916-920.

763 Choi, S. H., S. B. Mukasa, X.-H. Zhou, X. H. Xian, and A. V. Andronikov (2008), Mantle
764 dynamics beneath East Asia constrained by Sr, Nd, Pb and Hf isotopic systematics of ultramafic
765 xenoliths and their host basalts from Hannuoba, North China, *Chemical Geology*, *248*(1-2), 40-
766 61.

767 Choi, S. H., K. Suzuki, S. B. Mukasa, J. I. Lee, and H. Jung (2010), Lu-Hf and Re-Os
768 systematics of peridotite xenoliths from Spitsbergen, western Svalbard: Implications for mantle-
769 crust coupling, *Earth and Planetary Science Letters*, *297*(1-2), 121-132.

770 Cirilli, S., A. Marzoli, L. Tanner, H. Bertrand, N. Buratti, F. Jourdan, G. Bellieni, D. Kontak, and
771 P. R. Renne (2009), Latest Triassic onset of the Central Atlantic Magmatic Province (CAMP)
772 volcanism in the Fundy Basin (Nova Scotia): New stratigraphic constraints, *Earth and Planetary*
773 *Science Letters*, *286*, 514-525.

774 Coffin, M. F., and O. Eldholm (1992), Volcanism and continental break-up; a global compilation
775 of large igneous provinces, *Geological Society Special Publications*, *68*, 17-30.

776 Coltice, N., B. Phillips, H. Bertrand, Y. Ricard, and P. Rey (2007), Global warming of the
777 mantle at the origin of flood basalts over supercontinents, *Geology*, *35*(5), 391-394.

778 Courtillot, V., C. Jaupart, I. Manighetti, P. Tapponnier, and J. Besse (1999), On causal links
779 between flood basalts and continental breakup, *Earth and Planetary Science Letters*, *166*, 177-
780 195.

781 Davies, J. H. F. L., A. Marzoli, H. Bertrand, N. Youbi, M. Ernesto, and U. Schaltegger (2017),
782 End-Triassic mass extinction started by intrusive CAMP activity, *Nature Communications, 8,*
783 *15596*.

784 De Boer, J. (1992), Stress configurations during and following emplacement of ENA basalts in
785 the northern Appalachians, In *Eastern North American Mesozoic Magmatism*, Eds. Puffer, J.H.
786 and P.C. Ragland, *Special Papers-Geological Society of America, 268*, 361.

787 De Min, A., E. M. Piccirillo, A. Marzoli, G. Bellieni, P. R. Renne, M. Ernesto, and L. S.
788 Marques (2003), The Central Atlantic Magmatic Province (CAMP) in Brazil: petrology,
789 geochemistry, $^{40}Ar/^{39}Ar$ ages, paleomagnetism and geodynamic implications, *Geophysical*
790 *Monograph Series*, *136*, 91-128.

791 Deckart, K., G. Féraud, and H. Bertrand (1997), Age of Jurassic continental tholeiites of French
792 Guyana, Surinam and Guinea: Implications for the initial opening of the Central Atlantic Ocean,
793 *Earth and Planetary Science Letters*, *150*, 205-220.

794 Deckart, K., H. Bertrand, and J.-P. Liégeois (2005), Geochemistry and Sr, Nd, Pb isotopic
795 composition of the Central Atlantic Magmatic Province (CAMP) in Guyana and Guinea, *Lithos*,
796 *82*, 289-314.

797 Dorais, M. J., and M. Tubrett (2008), Identification of a subduction zone component in the
798 Higganum dike, Central Atlantic Magmatic Province: A LA-ICPMS study of clinopyroxene with
799 implications for flood basalt petrogenesis, *Geochemistry, Geophysics, Geosystems*, *9*(10).

800 Dorais, M. J., M. Harper, S. Larson, H. Nugroho, P. Richardson, and N. Roosmawati (2005), A
801 comparison of Eastern North America and Coastal New England magma suites: implications for
802 subcontinental mantle evolution and the broad-terrane hypothesis, *Canadian Journal Earth Sci*,
803 *42*(1571-1587).

804 Dostal, J., and C. Dupuy (1984), Geochemistry of the North Mountain Basalts (Nova Scotia,
805 Canada), *Chemical Geology*, *45*(3), 245-261.

806 Dostal, J., and M. Durning (1998), Geochemical constraints on the origin and evolution of early
807 Mesozoic dikes in Atlantic Canada, *European Journal Mineralogy*, *10*, 79-93.

808 Dunning, G. R., and J. P. Hodych (1990), U/Pb zircon and baddeleyite ages for the Palisades and
809 Gettysburg sills of the northeastern United States: Implications for the age of the
810 Triassic/Jurassic boundary, *Geology*, *18*, 795-798.

811 Dupuy, C., J. Marsh, J. Dostal, A. Michard, and S. Testa (1988), Asthenospheric and lithospheric
812 sources for Mesozoic dolerites from Liberia (Africa): trace element and isotopic evidence, *Earth*
813 *and Planetary Science Letters*, *87*(1), 100-110.

814 Eisele, J., M. Sharma, S. J. Galer, J. Blichert-Toft, C. W. Devey, and A. W. Hofmann (2002),
815 The role of sediment recycling in EM-1 inferred from Os, Pb, Hf, Nd, Sr isotope and trace
816 element systematics of the Pitcairn hotspot, *Earth and Planetary Science Letters*, *196*(3), 197-
817 212.

818 Ernst, R. E., and K. L. Buchan (2003), Recognizing Mantle Plumes in the Geological Record,
819 *Annual Reviews Earth Planetary Science*, *31*, 469-523.

820 Ernst, R. E., E. B. Grosfils, and D. Mège (2001), Giant Dike Swarms: Earth, Venus, and Mars,
821 *Annual Reviews Earth Planetary Science*, *29*, 489-534.

822 Falloon, T.J. and L.V. Danyushevsky (2000), Melting of refractory mantle at 1.5, 2 and 2.5 GPa
823 under anhydrous and H_2O-undersaturated conditions: Implications for the petrogenesis of high-
824 Ca boninites and the influence of subduction components on mantle melting, *Journal of*
825 *Petrology*, 41(2), 257-283.

826 Frisby, C., M. Bizimis, and S. Mallick (2016), Hf-Nd isotope decoupling in bulk abyssal
827 peridotites due to serpentinization, *Chemical Geology*, *440*, 60-72.

828 Garcon, M., C. Chauvel, C. France-Lanord, P. Huyghe, and J. Lave (2013), Continental
829 sedimentary processes decouple Nd and Hf isotopes, *Geochimica Et Cosmochimica Acta*, *121*,
830 177-195.

831 Garcon, M., C. Chauvel, C. France-Lanord, M. Limonta, and E. Garzanti (2014), Which minerals
832 control the Nd-Hf-Sr-Pb isotopic compositions of river sediments?, *Chemical Geology*, *364*, 42-
833 55.

834 Geldmacher, J., K. Hoernle, B. B. Hanan, J. Blichert-Toft, F. Hauff, J. B. Gill, and H.-U.
835 Schmincke (2011), Hafnium isotopic variations in East Atlantic intraplate volcanism,
836 *Contributions to Mineralogy and Petrology*, *162*(1), 21-36.

837 Gillard, M., D. Sauter, J. Tugend, S. Tomasi, M.-E. Epin, and G. Manatschal (2017), Birth of an
838 oceanic spreading center at a magma-poor rift system, *Scientific reports*, *7*(1), 15072.

839 Griffin, W., N. Pearson, E. Belousova, S. v. Jackson, E. Van Achterbergh, S. Y. O'Reilly, and S.
840 Shee (2000), The Hf isotope composition of cratonic mantle: LAM-MC-ICPMS analysis of
841 zircon megacrysts in kimberlites, *Geochimica et Cosmochimica Acta*, *64*(1), 133-147.

842 Guo, W., S. Zhao, F. Wang, Z. Yang, S. Jia, and Z. Liu (2019), Crustal structure of the eastern
843 Piedmont and Atlantic coastal plain in North Carolina and Virginia, eastern North American
844 margin, *Earth, Planets and Space*, *71*(1), 69.

845 Halliday, A. N., A. P. Dickin, R. N. Hunter, G. R. Davies, T. J. Dempster, P. J. Hamilton, and B.
846 G. Upton (1993), Formation and composition of the lower continental crust: evidence from
847 Scottish xenolith suites, *Journal of Geophysical Research: Solid Earth*, *98*(B1), 581-607.

848 Hames, W. E., P. R. Renne, and C. Ruppel (2000), New evidence for geologically instantaneous
849 emplacement of earliest Jurassic Central Atlantic magmatic province basalts on the North
850 American margin, *Geology*, *28*, 859-862.

851 Heatherington, A. L., and P. A. Mueller (1999), Lithospheric sources of North Florida, USA
852 tholeiites and implications for the origin of the Suwannee terrane, *Lithos*, *46*, 215-233.

853 Heimdal, T. H., H. H. Svensen, J. Ramezani, K. Iyer, E. Pereira, R. Rodrigues, M. T. Jones, and
854 S. Callegaro (2018), Large-scale sill emplacement in Brazil as a trigger for the end-Triassic
855 crisis, *Scientific Reports*, *8*, 141.

856 Heinonen, A., I. Mänttäri, O.T. Rämö, T. Andersen, and K. Larjamo (2016), A prior evidence for
857 zircon antecryst entrainment in megacrystic Proterozoic granites, *Geology*, *44*, 227-230.

858 Hermes, O. (1964), A quantitative petrographic study of dolerite in the Deep River Basin, North
859 Carolina, *Am. Mineral, 49*, 1718-1729.

860 Herzberg, C., and E. Gazel (2009), Petrological evidence for secular cooling in mantle plumes,
861 *Nature, 458*(7238), 619.

862 Hesselbo, S. P., S. A. Robinson, F. Surlyk, and S. Piasecki (2002), Terrestrial and marine
863 extinction at the Triassic-Jurassic boundary synchronized with major carbon-cycle perturbation:
864 A link to initiation of massive volcanism?, *Geology*, *30*(3), 251-254.

865 Hill, R. I. (1991), Starting plumes and continental break-up, *Earth and Planetary Science*
866 *Letters*, *104*(2), 398-416.

867 Hodych, J. P., and G. R. Dunning (1992), Did the Manicouagan impact trigger end-of-Triassic
868 mass extinction?, *Geology*, *20*, 51-54.

869 Holbrook, W., and P. Kelemen (1993), Large igneous province on the US Atlantic margin and
870 implications for magmatism during continental breakup, *Nature*, *364*(6436), 433-436.

871 Holbrook, W. S., E. Reiter, G. Purdy, D. Sawyer, P. Stoffa, J. Austin Jr, J. Oh, and J. Makris
872 (1994), Deep structure of the US Atlantic continental margin, offshore South Carolina, from
873 coincident ocean bottom and multichannel seismic data, *Journal of Geophysical Research*,
874 *99*(B5), 9155-9178.

875 Hole, M. J. (2015), The generation of continental flood basalts by decompression melting of
876 internally heated mantle, *Geology*, *43*(4), 311-314.

877 Holm, P.M., J.R. Wilson, B.P. Christensen, L. Hansen, S.L. Hansen, K.M. Hein, A.K.
878 Mortensen, R. Pedersen, S. Plesner, and M.K. Runge (2006), Sampling the Cape Verde Mantle
879 Plume: Evolution of melt compositions on Santo Antão, Cape Verde Islands. *Journal of*
880 *Petrology*, *47*, 145-189.

881 Huang, Y.-M., P. Van Calsteren, and C. I. Hawkesworth (1995), The evolution of the lithosphere
882 in southern Africa: a perspective on the basic granulite xenoliths from kimberlites in South
883 Africa, *Geochimica et Cosmochimica Acta*, *59*(23), 4905-4920.

884 Iacumin, M., A. De Min, E. M. Piccirillo, and G. Bellieni (2003), Source mantle heterogeneity
885 and its role in the genesis of Late Archaean-Proterozoic (2.7-1.0 Ga) and Mesozoic (200 and 130
886 Ma) tholeiitic magmatism in the South American Platform, *Earth-Science Reviews*, *62*, 365-397.

887 Ingle, S., P. A. Mueller, A. L. Heatherington, and M. Kozuch (2003), Isotopic evidence for the
888 magmatic and tectonic histories of the Carolina terrane: implications for stratigraphy and terrane
889 affiliation, *Tectonophysics*, *371*(1-4), 187-211.

890 Jackson, M.G., S.R. Hart, A.P. Koppers, H. Staudigel, J. Konter, J. Blusztajn, M. Kurz, and J.A.
891 Russell (2007), The return of subducted continental crust in Samoan lavas, *Nature*, 448, 684-687.

892 Jackson, M. G., and R. Dasgupta (2008), Compositions of HIMU, EM1, and EM2 from global
893 trends between radiogenic isotopes and major elements in ocean island basalts, *Earth and*
894 *Planetary Science Letters*, *276*(1-2), 175-186.

895 Jaffey, A. H., K. F. Flynn, Glendeni.Le, W. C. Bentley, and A. M. Essling (1971), Precision
896 Measurement of Half-Lives and Specific Activities of U-235 and U-238, *Physical Review C*,
897 *4*(5), 1889-1906.

898 Janney, P. E., and P. R. Castillo (2001), Geochemistry of the oldest Atlantic oceanic crust
899 suggests mantle plume involvement in the early history of the central Atlantic Ocean, *Earth and*
900 *Planetary Science Letters*, *192*, 291-302.

901 Janney, P., A. Le Roex, and R. Carlson (2005), Hafnium isotope and trace element constraints on
902 the nature of mantle heterogeneity beneath the central Southwest Indian Ridge (13 E to 47 E),
903 *Journal of Petrology*, *46*(12), 2427-2464.

904 Johnson, M. C., and T. Plank (2000), Dehydration and melting experiments constrain the fate of
905 subducted sediments, *Geochemistry, Geophysics, Geosystems*, *1*(12), doi:
906 10.1029/1999GC000014.

907 Jourdan, F., A. Marzoli, H. Bertrand, M. Cosca, and D. Fontignie (2003), The northernmost
908 CAMP: $^{40}Ar/^{39}Ar$ age, petrology and Sr-Nd-Pb isotope geochemistry of the Kerforne dike,
909 Brittany, France, *Geophysical Monograph Series*, *136*, 209-226.

910 Jourdan, F., H. Bertrand, U. Schärer, J. Blichert-Toft, G. Féraud, and A. B. Kampunzu (2007),
911 Major and trace element and Sr, Nd, Hf, and Pb isotope compositions of the Karoo Large
912 Igneous Province, Botswana-Zimbabwe: Lithosphere vs mantle plume contribution, *Journal of*
913 *Petrology*, *48*(6), 1043-1077.

914 Jourdan, F., A. Marzoli, H. Bertrand, S. Cirilli, L. H. Tanner, D. J. Kontak, G. McHone, P. R.
915 Renne, and G. Bellieni (2009), $^{40}Ar/^{39}Ar$ ages of CAMP in North America: Implications for the
916 Triassic-Jurassic boundary and the ^{40}K decay constant bias, *Lithos*, *110*, 167-180.

Kempton, P. D., H. Downes, and M. Lustrino (2018), Pb and Hf isotope evidence for mantle enrichment processes and melt interactions in the lower crust and lithospheric mantle in Miocene orogenic volcanic rocks from Monte Arcuentu (Sardinia, Italy), *Geosphere*, *14*(3), 926-950.

Kent, R. (1991), Lithospheric uplift in eastern Gondwana: Evidence for a long-lived mantle plume system?, *Geology*, *19*(1), 19-23.

Khanna, T., M. Bizimis, G. Yogodzinski, and S. Mallick (2014), Hafnium-neodymium isotope systematics of the 2.7 Ga Gadwal greenstone terrane, Eastern Dharwar craton, India: Implications for the evolution of the Archean depleted mantle, *Geochimica Et Cosmochimica Acta*, *127*, 10-24.

Klein, E. M. (2004), Geochemistry of the Igneous Ocean Crust, in *Treatise on Geochemistry*, edited by H. D. Holland and K. K. Turekian, pp. 433-463, Elsevier, Amsterdam.

Klügel, A., K. Galipp, K. Hoernle, F. Hauff, and S. Groom (2017), Geochemical and volcanological evolution of La Palma, Canary Islands. *Journal of Petrology, 58,* 1227-1248.

Knight, K. B., S. Nomade, P. R. Renne, A. Marzoli, H. Bertrand, and N. Youbi (2004), The Central Atlantic Magmatic Province at the Triassic-Jurassic boundary: paleomagnetic and $^{40}Ar/^{39}Ar$ evidence from Morocco for brief, episodic volcanism, *Earth and Planetary Science Letters*, *228*, 143-160.

Kogiso, T., Y. Tatsumi, and S. Nakano (1997), Trace element transport during dehydration processes in the subducted oceanic crust: 1. Experiments and implications for the origin of ocean island basalts, *Earth and Planetary Science Letters*, *148*(1-2), 193-205.

937 Kontak, D. J. (2008), On the edge of CAMP: Geology and volcanology of the Jurassic North
938 Mountain Basalt, Nova Scotia, *Lithos, 101*, 74-101.

939 Koptev, A., E. Calais, E. Burov, S. Leroy, and T. Gerya (2015), Dual continental rift systems
940 generated by plume–lithosphere interaction, *Nature Geoscience*, *8*(5), 388.

941 Linnen, R. L. (1998), The solubility of Nb-Ta-Zr-Hf-W in granitic melts with Li and Li + F;
942 constraints for mineralization in rare metal granites and pegmatites, *Economic Geology*, *93*,
943 1013-1025.

944 Lizarralde, D., and W. S. Holbrook (1997), US mid-Atlantic margin structure and early thermal
945 evolution, *Journal of Geophysical Research, 102*, 22.

946 Magni, V. and A. Király (2019), Delamination, Reference Module in Earth Systems and
947 Environmental Sciences, Elsevier.

948 Mallick, S., J. J. Standish, and M. Bizimis (2015), Constraints on the mantle mineralogy of an
949 ultra-slow ridge: Hafnium isotopes in abyssal peridotites and basalts from the 9-25ºE Southwest
950 Indian Ridge, *Earth and Planetary Science Letters*, *410*, 42-53.

951 Marsh, J. S. (1987), Basalt geochemistry and tectonic discrimination within continental flood
952 basalt provinces, *Journal of Volcanology and Geothermal Research*, *32*(1-3), 35-49.

953 Marzoli, A., P. R. Renne, E. M. Piccirillo, M. Ernesto, G. Bellieni, and A. De Min (1999),
954 Extensive 200-Million-Year-Old Continental Flood Basalts of the Central Atlantic Magmatic
955 Province, *Science*, *284*, 616-618.

Marzoli, A., H. Bertrand, K.B. Knight, S. Cirilli, C. Verati, S. Nomade, P.R. Renne, N. Youbi, R. Martini, K. Allenbach, R. Neuwerth, C. Rapaille, L. Zaninetti, and G. Bellieni (2004), Synchrony of the Central Atlantic magmatic province and the Triassis-Jurassic boundary climatic and biotic crisis, *Geology*, *32*, 973-976.

Marzoli, A., F. Jourdan, J. H. Puffer, T. Cuppone, L. H. Tanner, R. E. Weems, H. Bertrand, S. Cirilli, G. Bellieni, and A. De Min (2011), Timing and duration of the Central Atlantic magmatic province in the Newark and Culpeper basins, eastern U.S.A., *Lithos*, *122*, 175-188.

Marzoli, A., F. Jourdan, F. Bussy, M. Chiaradia, and F. Costa (2014), Petrogenesis of tholeiitic basalts from the Central Atlantic magmatic province as revealed by mineral major and trace elements and Sr isotopes, *Lithos*, *188*, 44-59.

Marzoli, A., S. Callegaro, J. Dal Corso, J. H. F. L. Davies, M. Chiaradia, N. Youbi, H. Bertrand, L. Reisberg, R. Merle, and F. Jourdan (2018), The Central Atlantic Magmatic Province (CAMP): A Review, in *The Late Triassic World: Earth in a Time of Transition*, edited by L. H. Tanner, pp. 91-125, Springer International Publishing, Cham.

Marzoli, A., H. Bertrand, N. Youbi, S. Callegaro, R. Merle, L. Reisberg, M. Chiaradia, S. Brownlee, F. Jourdan, and A. Zanetti (2019), The Central Atlantic magmatic province (CAMP) in Morocco, *Journal of Petrology*, *60*, 945-996.

Mauche, R., G. Faure, L. M. Jones, and J. Hoefs (1989), Anomalous isotopic compositions of Sr, Ar and O in the Mesozoic diabase dikes of Liberia, West Africa, *Contributions to Mineralogy and Petrology*, *101*(1), 12-18.

May, P. R. (1971), Pattern of Triassic-Jurassic Diabase Dikes around the North Atlantic in the Context of Predrift Position of the Continents, *Geological Society of America Bulletin*, *82*, 1285-1292.

Mazza, S. E., E. Gazel, E. A. Johnson, M. Bizimis, R. McAleer, and C. B. Biryol (2017), Post-rift magmatic evolution of the eastern North American "passive-aggressive" margin, *Geochemistry, Geophysics, Geosystems*, *18*(1), 3-22.

Mazza, S. E., E. Gazel, M. Bizimis, R. Moucha, P. Béguelin, E. A. Johnson, R. J. McAleer, and A. V. Sobolev (2019), Sampling the volatile-rich transition zone beneath Bermuda, *Nature*, *569*(7756), 398.

McHone, J. G. (1978), Distribution, orientations, and ages of mafic dikes in central New England, *Geological Society of America Bulletin*, *89*(11), 1645-1655.

McHone, G. (1996), Broad-terrane Jurassic flood basalts across northeastern North America, *Geology*, *24*, 319-322.

McHone, J. G. (2000), Non-plume magmatism and rifting during the opening of the central Atlantic Ocean, *Tectonophysics*, *316*, 287-296.

McKenzie, D., and R. O'Nions (1991), Partial Melt Distributions From Inversion Of Rare-Earth Element Concentrations, *Journal of Petrology*, *32*, 1021.

993 Merle, R., A. Marzoli, H. Bertrand, L. Reisberg, C. Verati, C. Zimmermann, M. Chiaradia, and
994 G. Bellieni (2011), $^{40}Ar/^{39}Ar$ ages and Sr-Nd-Pb-Os geochemistry of CAMP tholeiites from
995 Western Maranhao basin (NE Brazil), *Lithos*, *122*, 137-151.

996 Merle, R., A. Marzoli, L. Reisberg, H. Bertrand, A. Nemchin, M. Chiaradia, S. Callegaro, F.
997 Jourdan, G. Bellieni, D. Kontak, J. Puffer, and J.G. McHone (2014), Sr, Nd, Pb and Os Isotope
998 Systematics of CAMP Tholeiites from Eastern North America (ENA): Evidence of a
999 Subduction-enriched Mantle Source, *Journal of Petrology*, *55*(1), 133-180.

1000 Morgan, P. (1983), Constraints on rift thermal processes from heat flow and uplift,
1001 *Tectonophysics*, *94*(1), 277-298.

1002 Münker, C., S. Weyer, E. Scherer, and K. Mezger (2001), Separation of high field strength
1003 elements (Nb, Ta, Zr, Hf) and Lu from rock samples for MC-ICPMS measurements, *Geochem.*
1004 *Geophys. Geosyst.*, *2*(12), doi: 10.1029/2001GC000183.

1005 Nehring, F., S.F. Foley, and P. Hölttä (2010), Trace element partitioning in the granulite facies,
1006 *Contrib. Mineral. Petrol.*, 159, 493-519.

1007 Nomade, S., K. Knight, E. Beutel, P. Renne, C. Verati, G. Féraud, A. Marzoli, N. Youbi, and H.
1008 Bertrand (2007), Chronology of the Central Atlantic Magmatic Province: Implications for the
1009 Central Atlantic rifting processes and the Triassic-Jurassic biotic crisis, *Palaeogeography,*
1010 *Palaeoclimatology, Palaeoecology*, *244*(1), 326-344.

1011 Oyarzun, R., M. Doblas, J. López-Ruiz, and J. M. Cebría (1997), Opening of the central Atlantic
1012 and asymmetric mantle upwelling phenomena: implications for long-lived magmatism in western
1013 North Africa and Europe, *Geology*, *25*(8), 727-730.

1014 Papezik, V., J. D. Greenough, J. A. Colwell, and T. J. Mallinson (1988), North Mountain basalt
1015 from Digby, Nova Scotia: models for a fissure eruption from stratigraphy and petrochemistry,
1016 *Canadian Journal of Earth Sciences*, *25*(1), 74-83.

1017 Pe-Piper, G., and D. J. W. Piper (1999), Were Jurassic tholeiitic lavas originally widespread in
1018 southeastern Canada?: a test of the broad terrane hypothesis, *Canadian Journal of Earth*
1019 *Sciences*, *36*(9), 1509-1516.

1020 Pegram, W. J. (1990), Development of continental lithospheric mantle as reflected in the
1021 chemistry of the Mesozoic Appalachian tholeiites, USA, *Earth and Planetary Science Letters*,
1022 *97*(3), 316-331.

1023 Pettingill, H. S., A. Sinha, and M. Tatsumoto (1984), Age and origin of anorthosites,
1024 charnockites, and granulites in the central Virginia Blue Ridge: Nd and Sr isotopic evidence,
1025 *Contributions to Mineralogy and Petrology*, *85*(3), 279-291.

1026 Plank, T., and C. H. Langmuir (1998), The chemical composition of subducting sediment and its
1027 consequences for the crust and mantle, *Chemical geology*, *145*(3), 325-394.

1028 Puffer, J. (1992), Eastern North American flood basalts in the context of the incipient breakup of
1029 Pangea, , In *Eastern North American Mesozoic Magmatism*, Eds. Puffer, J.H. and P.C. Ragland,
1030 *Special Papers-Geological Society of America*, v. 268, 95.

1031 Puffer, J. (2001), Contrasting high field strength element contents of continental flood basalts
1032 from plume versus reactivated-arc sources, *Geology*, *29*(8), 675-678.

1033 Puffer, J. H. (2003), A reactivated back-arc source for CAMP magma, *Geophysical Monograph*
1034 *Series, 136*, 151-162.

1035 Puffer, J., D. Hurtubise, F. Geiger, and P. Lechler (1981), Chemical composition and
1036 stratigraphic correlation of the Mesozoic basalt units of the Newark Basin, New Jersey, and the
1037 Hartford Basin, Connecticut, *Geological Society of America Bulletin*, *92*, 515-553.

1038 Ragland, P., L. Cummins, and J. Arthur (1992), Compositional patterns for early Mesozoic
1039 diabases from South Carolina to central Virginia, In *Eastern North American Mesozoic*
1040 *Magmatism,* Eds. Puffer, J.H. and P.C. Ragland, *Special Papers-Geological Society of America*,
1041 v. 268, 309.

1042 Reinemund, J. A. (1955), *Geology of the Deep River coal field, North Carolina,* Geological
1043 Survey Professional Paper 246, U.S. Government Printing Office, Washington, D.C.

1044 Rey, P. F. (2015), The geodynamics of mantle melting, *Geology*, *43*(4), 367-368.

1045 Ruiz-Martínez, V. C., T. H. Torsvik, D. J. J. van Hinsbergen, and C. Gaina (2012), Earth at
1046 200Ma: Global palaeogeography refined from CAMP palaeomagnetic data, *Earth and Planetary*
1047 *Science Letters*, *331*, 67-79.

1048 Salters, V. J. M., and S. R. Hart (1989), The Hafnium Paradox and the Role of Garnet in the
1049 Source of Mid-Ocean-Ridge Basalts, *Nature*, *342*(6248), 420-422.

1050 Salters, V. J., and A. Stracke (2004), Composition of the depleted mantle, *Geochemistry,*
1051 *Geophysics, Geosystems*, *5*(5), doi: 10.1029/2003GC000597.

Salters, V. J., J. Blichert-Toft, Z. Fekiacova, A. Sachi-Kocher, and M. Bizimis (2006), Isotope and trace element evidence for depleted lithosphere in the source of enriched Ko'olau basalts, *Contributions to Mineralogy and Petrology*, *151*(3), 297-312.

Salters, V. J., S. Mallick, S. R. Hart, C. E. Langmuir, and A. Stracke (2011), Domains of depleted mantle: New evidence from hafnium and neodymium isotopes, *Geochemistry, Geophysics, Geosystems*, *12*(8), doi: 10.1029/2011GC003617.

Saunders, A. D., S. M. Jones, L. A. Morgan, K. L. Pierce, M. Widdowson, and Y. G. Xu (2007), Regional uplift associated with continental large igneous provinces; the roles of mantle plumes and the lithosphere, *Chemical Geology*, *241*(3-4), 282-318.

Schmitz, M. D., J. D. Vervoort, S. A. Bowring, and P. J. Patchett (2004), Decoupling of the Lu-Hf and Sm-Nd isotope systems during the evolution of granulitic lower crust beneath southern Africa, *Geology*, *32*(5), 405-408.

Sebai, A., G. Feraud, H. Bertrand, and J. Hanes (1991), $^{40}Ar/^{39}Ar$ dating and geochemistry of tholeiitic magmatism related to the early opening of the Central Atlantic Rift, *Earth and Planetary Science Letters*, *104*(2), 455-472.

Sengör, A., and K. Burke (1978), Relative timing of rifting and volcanism on Earth and its tectonic implications, *Geophysical Research Letters*, *5*(6), 419-421.

Shaw, J., J. Baker, A. Kent, K. Ibrahim, and M. Menzies (2007), The geochemistry of the Arabian lithospheric mantle—a source for intraplate volcanism?, *Journal of Petrology*, *48*(8), 1495-1512.

Shellnutt, J. G., J. Dostal, and M.-W. Yeh (2018), Mantle source heterogeneity of the Early Jurassic basalt of eastern North America, *International Journal of Earth Sciences*, *107*(3), 1033-1058.

Sinha, A., J. Hogan, and J. Parks (1996), Lead Isotope Mapping of Crustal Reservoirs Within the Grenville Supertereane: I. Central and Southern Appalachians, *Geophysical Monograph-American Geophysical Union*, *95*, 293-306.

Sobolev, S. V., A. V. Sobolev, D. V. Kuzmin, N. A. Krivolutskaya, A. G. Petrunin, N. T. Arndt, V. A. Radko, and Y. R. Vasiliev (2011), Linking mantle plumes, large igneous provinces and environmental catastrophes, *Nature*, *477*(7364), 312-316.

Söderlund, U., P. J. Patchett, J. D. Vervoort, and C. E. Isachsen (2004), The ^{176}Lu decay constant determined by Lu–Hf and U–Pb isotope systematics of Precambrian mafic intrusions, *Earth and Planetary Science Letters*, *219*(3-4), 311-324.

Spera, F. J., and W. A. Bohrson (2001), Energy-constrained open-system magmatic processes I: General model and energy-constrained assimilation and fractional crystallization (EC-AFC) formulation, *Journal of Petrology*, *42*(5), 999-1018.

Staudigel, H., T. Plank, B. White, and H. U. Schmincke (1996), Geochemical fluxes during seafloor alteration of the basaltic upper oceanic crust: DSDP Sites 417 and 418, *Subduction: top to bottom*, *96*, 19-38.

Stracke, A., M. Bizimis, and V. J. M. Salters (2003), Recycling oceanic crust: Quantitative constraints, *Geochemistry, Geophysics, Geosystems*, *4*(3), 8003.

1092 Taylor, S. R., and S. M. McLennan (1995), The geochemical evolution of the continental crust,
1093 *Reviews of Geophysics*, *33*(2), 241-265.

1094 Tollo, R., and D. Gottfried (1992), Petrochemistry of Jurassic basalt from eight cores, Newark
1095 basin, New Jersey, In *Eastern North American Mesozoic Magmatism*, Eds. Puffer, J.H. and P.C.
1096 Ragland, *Special Papers-Geological Society of America*, v. 268, 233.

1097 Verati, C., H. Bertrand, and G. Féraud (2005), The farthest record of the Central Atlantic
1098 Magmatic Province into West Africa craton: Precise $^{40}Ar/^{39}Ar$ dating and geochemistry of
1099 Taoudenni basin intrusives (northern Mali), *Earth and Planetary Science Letters*, *235*(1), 391-
1100 407.

1101 Verati, C., C. Rapaille, G. Féraud, A. Marzoli, H. Bertrand, and N. Youbi (2007), $^{40}Ar/^{39}Ar$ ages
1102 and duration of the Central Atlantic Magmatic Province volcanism in Morocco and Portugal and
1103 its relation to the Triassic-Jurassic boundary, *Palaeogeography, Palaeoclimatology,*
1104 *Palaeoecology*, *244*(1), 308-325.

1105 Vervoort, J. D., P. J. Patchett, J. Blichert-Toft, and F. Albarede (1999), Relationships between
1106 Lu-Hf and Sm-Nd isotopic systems in the global sedimentary system, *Earth and Planetary*
1107 *Science Letters*, *168*(1-2), 79-99.

1108 Vervoort, J. D., P. J. Patchett, F. Albarede, J. Blichert-Toft, R. Rudnick, and H. Downes (2000),
1109 Hf-Nd isotopic evolution of the lower crust, *Earth and Planetary Science Letters*, *181*(1-2), 115-
1110 129.

1111 Vervoort, J. D., T. Plank, and J. Prytulak (2011), The Hf-Nd isotopic composition of marine
1112 sediments, *Geochimica Et Cosmochimica Acta*, *75*, 5903-5926.

1113 Wedepohl, K. H. (1995), The composition of the continental crust, *Geochimica et cosmochimica*
1114 *Acta*, *59*(7), 1217-1232.

1115 Weigand, P. W., and P. C. Ragland (1970), Geochemistry of Mesozoic dolerite dikes from
1116 eastern North America, *Contributions to Mineralogy and Petrology*, *29*(3), 195-214.

1117 Whalen, L., E. Gazel, C. Vidito, J. Puffer, M. Bizimis, W. Henika, and M. J. Caddick (2015),
1118 Supercontinental inheritance and its influence on supercontinental breakup: The Central Atlantic
1119 Magmatic Province and the breakup of Pangea, *Geochemistry Geophysics Geosystems*, *16*(10),
1120 3532-3554.

1121 White, R. S., and D. P. McKenzie (1989), Volcanism at Rifts, *Scientific American*, *261*(1), 62-
1122 71.

1123 Willbold, M., and A. Stracke (2006), Trace element composition of mantle end-members:
1124 Implications for recycling of oceanic and upper and lower continental crust, *Geochem. Geophys.*
1125 *Geosyst.*, *7*(4), doi: 10.1029/2005GC001005.

1126 Wilson, J. T. (1966), Did the Atlantic close and then re-open?, *Nature*, *211*, 676-681.

1127 Wilson, M. (1997), Thermal evolution of the Central Atlantic passive margins: continental
1128 break-up above a Mesozoic super-plume, *Journal of the Geological Society*, *154*(3), 491-495.

1129 Wittig, N., J. A. Baker, and H. Downes (2007), U–Th–Pb and Lu–Hf isotopic constraints on the
1130 evolution of sub-continental lithospheric mantle, French Massif Central, *Geochimica et*
1131 *Cosmochimica Acta*, *71*(5), 1290-1311.

1132 Wittig, N., D. G. Pearson, S. Duggen, J. A. Baker, and K. Hoernle (2010), Tracing the
1133 metasomatic and magmatic evolution of continental mantle roots with Sr, Nd, Hf and and Pb
1134 isotopes: A case study of Middle Atlas (Morocco) peridotite xenoliths, *Geochimica Et*
1135 *Cosmochimica Acta*, *74*(4), 1417-1435.

1136 Woodhead, J. D., and C. W. Devey (1993), Geochemistry of the Pitcairn seamounts, I: source
1137 character and temporal trends, *Earth and Planetary Science Letters*, *116*(1-4), 81-99.

1138 Workman, R. K., and S. R. Hart (2005), Major and trace element composition of the depleted
1139 MORB mantle (DMM), *Earth and Planetary Science Letters*, *231*, 53-72.

1140 Workman, R. K., S. R. Hart, M. Jackson, M. Regelous, K. Farley, J. Blusztajn, M. Kurz, and H.
1141 Staudigel (2004), Recycled metasomatized lithosphere as the origin of the Enriched Mantle II
1142 (EM2) end-member: Evidence from the Samoan Volcanic Chain, *Geochemistry, Geophysics,*
1143 *Geosystems*, *5*(4), doi: 10.1029/2003GC000623.

1144 Wysoczanski, R., J. Gamble, P. Kyle, and M. Thirlwall (1995), The petrology of lower crustal
1145 xenoliths from the Executive Committee Range, Marie Byrd Land volcanic province, West
1146 Antarctica, *Lithos*, *36*(3-4), 185-201.

1147 Zartman, R. E., P. D. Kempton, J. B. Paces, H. Downes, I. S. Williams, G. Dobosi, and K. Futal
1148 (2013), Lower-crustal xenoliths from Jurassic kimberlite diatremes, Upper Michigan (USA):
1149 Evidence for Proterozoic Orogenesis and plume magmatism in the lower crust of the Southern
1150 Superior Province, *Journal of Petrology*, *54*, 575-608.

1151 Zhao, S., and W. Guo (2019), Crustal Structure of Eastern North Carolina: Piedmont and Coastal
1152 Plain, *Bulletin of the Seismological Society of America*, *109*(6), 2288-2304.

1153

1154 **FIGURE CAPTIONS**

1155 Figure 1. Tectonic reconstruction of the central Atlantic region around the time of CAMP
1156 emplacement, with Southern and Northern ENA, Morocco, and Sierra Leone sample locations
1157 for this study indicated. Lines and fields in red and blue show the locations of CAMP intrusions
1158 and lava flows, as indicated in the legend (after Deckart et al., 2005, Marzoli et al., 2018).
1159 Indicated groupings within CAMP refer to magma categories defined by Marzoli et al. (2018).

1160 Figure 2. Age-corrected isotope results for samples analyzed in this study, with comparative
1161 values from the literature, for **a.** $\varepsilon_{Hf\ 201Ma}$ vs. $\varepsilon_{Nd\ 201Ma}$, **b.** $\varepsilon_{Hf\ 201Ma}$ vs. $^{206}Pb/^{204}Pb_{201Ma}$, and **c.**
1162 $^{207}Pb/^{204}Pb_{201Ma}$ vs. $^{206}Pb/^{204}Pb_{201Ma}$. Lead and $\varepsilon_{Nd\ 201Ma}$ isotope data for samples in this study are
1163 from Callegaro et al. (2013, 2017) and Merle et al. (2014). Other literature data for CAMP are
1164 from Callegaro et al. (2013, 2014, 2017), Deckart et al. (2005), Jourdan et al. (2003), Marzoli et
1165 al. (2019), Merle et al. (2011, 2014), and Whalen et al. (2015), with regional groups defined after
1166 Whalen et al. (2015). End members are shown as black squares, with values as in Table S1 and
1167 described in the text; "GLOSS" refers to global average subducted sediment after Plank and
1168 Langmuir (1998) and Chauvel et al. (2008), aged 170 Ma to represent Paleozoic subducted
1169 sediments (that is, assuming a subduction recycling age of ~370 Ma sampled by CAMP melting
1170 at ~200 Ma, after Callegaro et al. (2013) and Whalen et al. (2015)), "UCC" refers to the average
1171 composition of upper continental crust from the Carolina terrane, "Mafic LCC" and
1172 "Intermediate LCC" refer to Proterozoic mafic and intermediate-SiO_2 lower continental crust

compositions, as described in the text and Table S2, and the "Geochron" line shows the composition of the geochron corrected to an age of 201 Ma. Also shown for reference are the ε_{Hf} vs. ε_{Nd} mantle array (Vervoort et al., 2011), the field of MORB (Chauvel et al., 2008), the field of Hawaiian lavas (Blichert-Toft et al., 1999), the global seawater array and the field of ferromanagese nodules (after Albarede et al., 1998), average marine sediments from Chauvel et al. (2014) and Plank and Langmuir (1998), and the field of Karoo LIP basalts (Jourdan et al., 2007), which exhibits a shallow sloping trend similar to Hawaiian basalts and our ENA CAMP array. The composition of average Atlantic OIB is after Marzoli et al. (2019) and references therein, e.g. Cape Verde data from Holm et al. (2006) and Canary Islands data from Klügel et al. (2017). Data sets and compositions unrelated to CAMP are plotted for reference and have not been age-corrected, except where indicated in the text or data tables. End-member, age-corrected isotopic compositions for EM-1, EM-2, and DMM were calculated using the compositions shown in Table S1.

Figure 3. **a.** $\varepsilon_{Hf\ 201Ma}$ vs. $\varepsilon_{Nd\ 201Ma}$ and **b.** $\varepsilon_{Hf\ 201Ma}$ vs. $^{206}Pb/^{204}Pb_{201Ma}$ diagrams for samples from this study, showing calculated EC-AFC trajectories after Bohrson and Spera (2001) and Spera and Bohrson (2001), as described in the text and using values from Table S1. Trajectories are shown for a parent basalt composition similar to sample CS49, which has the most incompatible element depleted composition based on radiogenic isotope compositions (yellow star; Table 2), with hypothesized compositions for several upper and lower continental crust assimilants described in the text and shown in Table S2. The assimilants shown are 1) averaged Carolina terrane upper continental crust ("Carolina UCC"); 2) a Proterozoic lower crustal mafic granulite ("Mafic LCC"); and 3) an intermediate lower continental granulite with a hypothesized $^{206}Pb/^{204}Pb_{201Ma}$ ratio of 17.3, after the discussion in the text ("Intermediate LCC"). Upper

continental crust was calculated using mean compositions of measured Carolina terrane crustal rocks from Pettingill et al. (1984) and Sinha et al. (1996) and the data compilation of Whalen et al. (2015). Carolina terrane crustal data set lacks hafnium isotope measurements, so UCC $\varepsilon_{Hf\ 201Ma}$ values were then calculated assuming a relationship with $\varepsilon_{Nd\ 201Ma}$ along the terrestrial array (Vervoort et al., 1999) (Table S1). The Proterozoic mafic granulite shown has elevated Lu/Hf ratios, similar to average mafic xenoliths from Michigan (Zartman et al., 2013) and representative of mafic LCC with decoupled ε_{Hf} and ε_{Nd}. In panel (b), we additionally test mafic LCC with an alternative Pb isotope composition more closely resembling comparable mafic granulite xenoliths from Markt, South Africa (Huang et al., 1995) ("Markt LCC"). Intermediate granulites may have isotopic signatures that record higher time-integrated incompatible element concentrations than mafic basement (i.e., less radiogenic $^{143}Nd/^{144}Nd$ and $^{176}Hf/^{177}Hf$ ratios), so the intermediate LCC composition has a relatively incompatible element-enriched composition within the range of xenolith measurements by Schmitz et al. (2004). For our intermediate-SiO_2 granulite composition, we also determined partitioning behavior using mineral modes similar to the intermediate-SiO_2 xenolith sampled by Zartman et al (2013). Tickmarks indicate the percentage of crustal assimilant added to the magma, up to a maximum of 10% addition. All other symbols and lines as in Figure 2.

Figure 4. Ternary mixing diagrams for partial melts of DMM, EM-1, and EM-2 sources, as defined in Table S1 and the text, for a. $\varepsilon_{Hf\ 201Ma}$ vs. $\varepsilon_{Nd\ 201Ma}$, b. $\varepsilon_{Hf\ 201Ma}$ vs. $^{206}Pb/^{204}Pb_{201Ma}$, and c. $^{207}Pb/^{204}Pb_{201Ma}$ vs. $^{206}Pb/^{204}Pb_{201Ma}$. Mixing lines are plotted in 10% increments; symbols, lines, and mixing reservoirs as in Figure 2. Mantle reservoirs used for the mixing calculations use relatively recent estimates for the isotopic composition of enriched mantle sources (e.g., Jackson and Dasgupta, 2008; Jackson et al., 2007), resulting in different values than prior

studies; however, the results confirm that mixing of these reservoirs fails to explain southern ENA CAMP (Callegaro et al., 2013). More recent research (e.g., Marzoli et al., 2019) suggests that CAMP asthenosphere was in fact less depleted than global DMM and may more closely resemble the PREMA reservoir (Zindler and Hart, 1986), but our mixing trajectories show that the enriched melting end-members are mainly responsible for the observed mismatch, not the depleted end-member.

Figure 5. Ternary mixing diagrams for solid DMM, EM-1, and EM-2 source reservoirs, as defined in Table S1 and the text, for a. $\varepsilon_{Hf\ 201Ma}$ vs. $\varepsilon_{Nd\ 201Ma}$, b. $\varepsilon_{Hf\ 201Ma}$ vs. $^{206}Pb/^{204}Pb_{201Ma}$, and c. $^{207}Pb/^{204}Pb_{201Ma}$ vs. $^{206}Pb/^{204}Pb_{201Ma}$. Mixing lines are plotted in 10% increments; symbols, lines, and mixing reservoirs as in Figure 2.

Figure 6. Ternary mixing diagrams for DMM melts, average Carolina terrane continental crust, and average subducted pelagic marine sediments (GLOSS), as defined in Table S1 and the text, for **a.** $\varepsilon_{Hf\ 201Ma}$ vs. $\varepsilon_{Nd\ 201Ma}$, **b.** $\varepsilon_{Hf\ 201Ma}$ vs. $^{206}Pb/^{204}Pb_{201Ma}$, and **c.** $^{207}Pb/^{204}Pb_{201Ma}$ vs. $^{206}Pb/^{204}Pb_{201Ma}$. Mixing lines are plotted in 10% increments; other symbols, lines, and mixing reservoirs as in Figure 2.

Figure 7. Isotope diagrams showing results of isotopic evolution and partial melting calculations for modified mantle wedge, for **a.** $\varepsilon_{Hf\ 201Ma}$ vs. $\varepsilon_{Nd\ 201Ma}$, **b.** $\varepsilon_{Hf\ 201Ma}$ vs. $^{206}Pb/^{204}Pb_{201Ma}$, and **c.** $^{207}Pb/^{204}Pb_{201Ma}$ vs. $^{206}Pb/^{204}Pb_{201Ma}$ and with symbols and lines as in Figure 2. The trajectories shown indicate calculated mantle compositions for a crustal recycling subduction and metasomatism age of 370 Ma and subsequent mantle melting at 201 Ma. Blue solid lines indicate mantle compositions when metasomatized by a mixture of fluid derived from altered oceanic crust (AOC) and fluid derived from subducted global oceanic sediment; "% Sed Fluid" labels

indicate the percentage of sediment-derived fluid in the metasomatizing fluid mixture. Red solid lines indicate the same, but for AOC-derived fluid and sediment-derived partial melts (with corresponding "% Sed Melt" labels). Dashed lines and associated labels indicate the amount of fluid added to the mantle during metasomatism up to 10% addition, as a mass fraction relative to the initial mantle material (0.01 to 0.10). We note that all fractions of added fluid from 1-10% addition are compressed into a single narrow zone in panel **c** and so are not labeled. See Table S4 for additional modeling details.

Figure 8. Diagrams showing mixing trajectories between recycled continental crustal rocks and partial melts of modified, metasomatized mantle, for **a.** $\varepsilon_{Hf\ 201Ma}$ vs. $\varepsilon_{Nd\ 201Ma}$, **b.** $\varepsilon_{Hf\ 201Ma}$ vs. $^{206}Pb/^{204}Pb_{201Ma}$, and **c.** $^{207}Pb/^{204}Pb_{201Ma}$ vs. $^{206}Pb/^{204}Pb_{201Ma}$ and with mixing lines in 10% increments and all other symbols as in Figure 2. The "modified mantle" mixing end member is a calculated 6% batch melt of mantle metasomatized using the methods described in the text and shown in Figure 7 and Table S4. The example case shown is for mantle modified by 7% addition of a fluid derived 25% from AOC and 75% from subducted sediments, with a 370 Ma recycling age and 201 Ma melting age. The UCC composition shown is local Carolina terrane, and the LCC composition is the "Markt mafic granulite" composition, both from Table S1.

Figure 1.

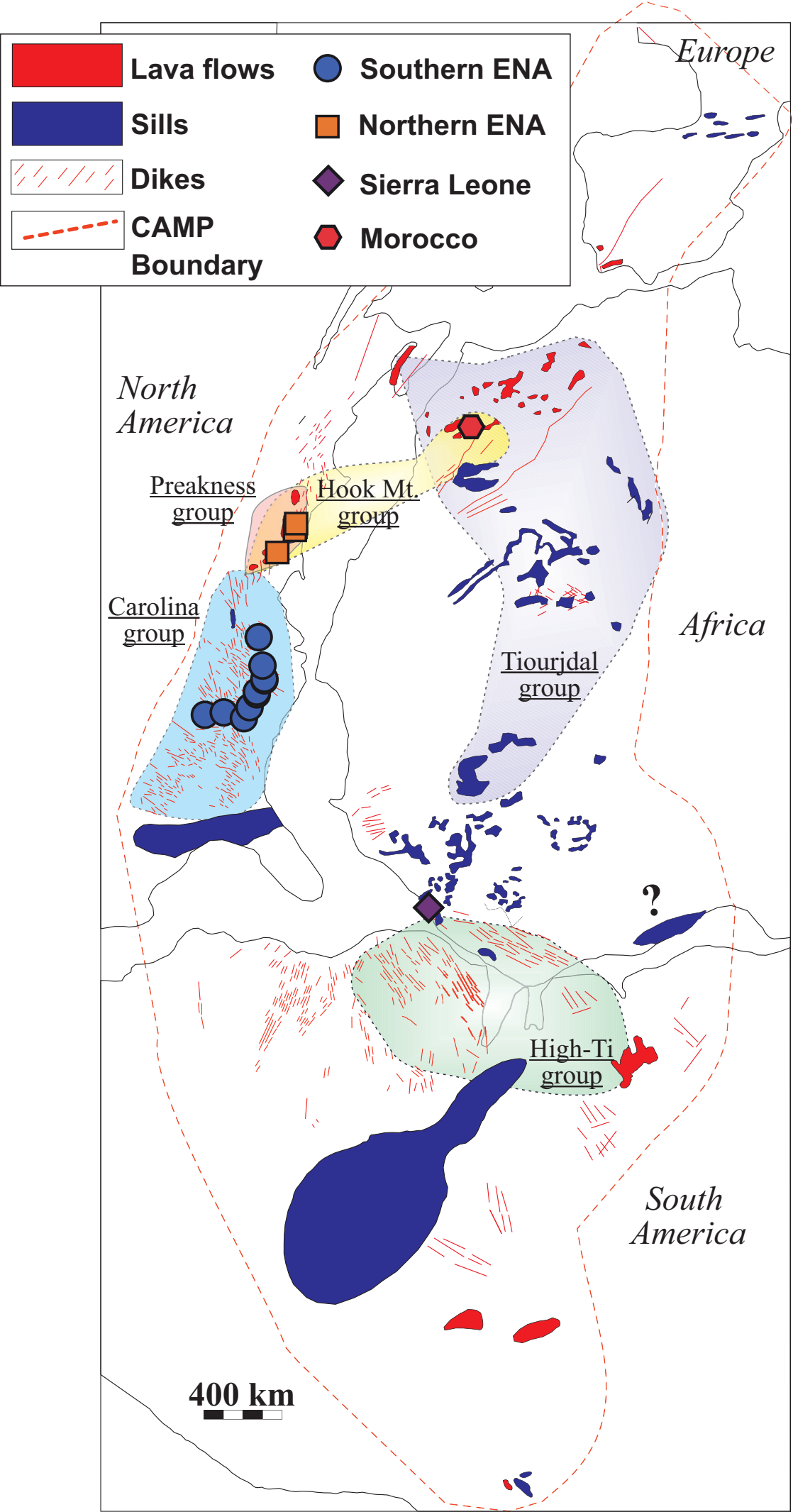
Lava flows
Sills
Dikes
CAMP Boundary
Southern ENA
Northern ENA
Sierra Leone
Morocco
Europe
North America
Preakness group
Hook Mt. group
Carolina group
Tiourjdal group
Africa
?
High-Ti group
South America
400 km

Figure 2.

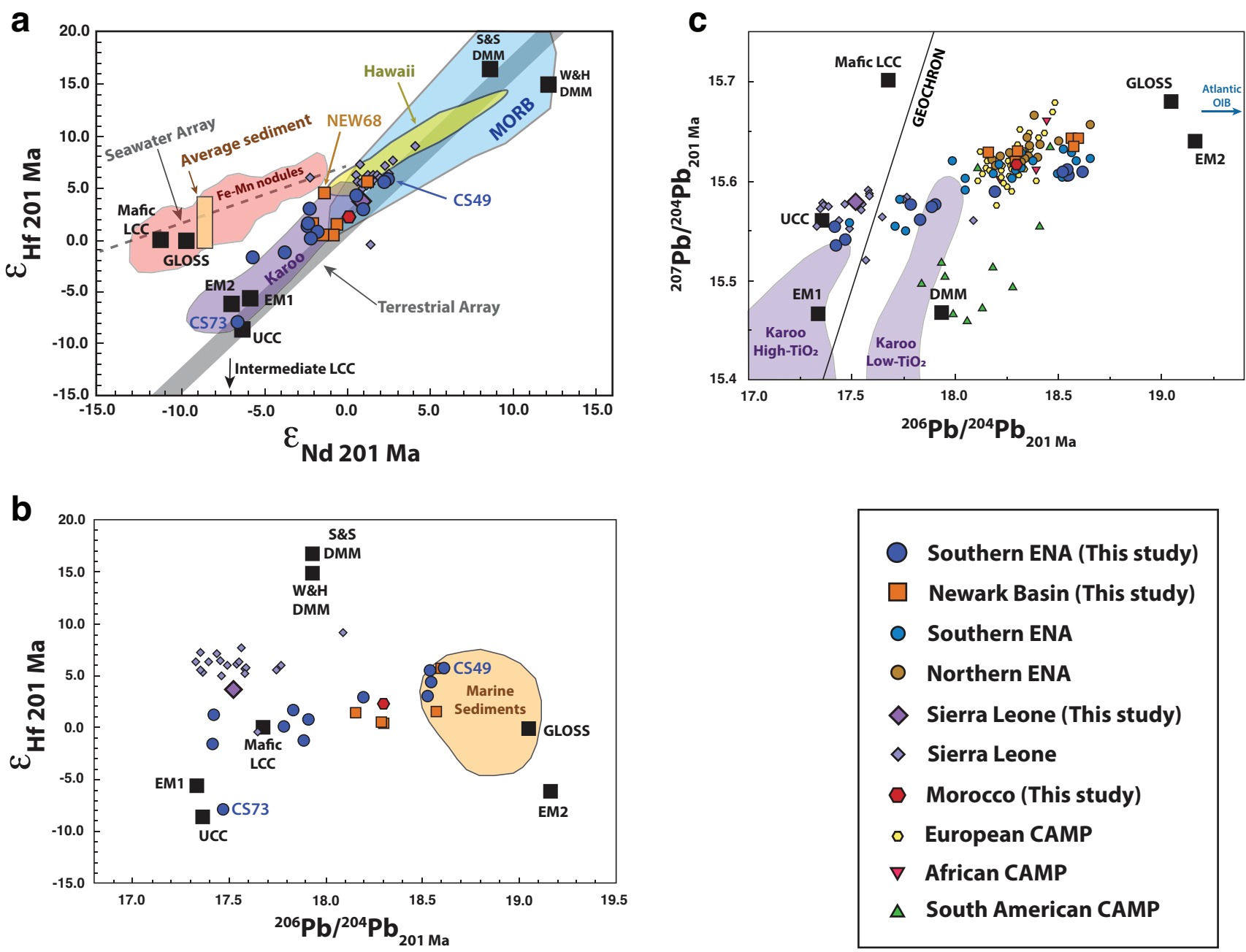
a
20.0
15.0
10.0
5.0
0.0
-5.0
-10.0
-15.0
-15.0
-10.0
-5.0
0.0
5.0
10.0
15.0
εHf 201 Ma
εNd 201 Ma
S&S DMM
W&H DMM
Hawaii
MORB
NEW68
Average sediment
Seawater Array
Fe-Mn nodules
Mafic LCC
GLOSS
CS49
Karoo
EM2
EM1
CS73
UCC
Terrestrial Array
Intermediate LCC
b
20.0
15.0
10.0
5.0
0.0
-5.0
-10.0
-15.0
17.0
17.5
18.0
18.5
19.0
19.5
εHf 201 Ma
206Pb/204Pb 201 Ma
S&S DMM
W&H DMM
CS49
Marine Sediments
GLOSS
Mafic LCC
EM1
CS73
UCC
EM2
c
15.7
15.6
15.5
15.4
17.0
17.5
18.0
18.5
19.0
207Pb/204Pb 201 Ma
206Pb/204Pb 201 Ma
Mafic LCC
GEOCHRON
GLOSS
Atlantic OIB
EM2
UCC
EM1
DMM
Karoo High-TiO2
Karoo Low-TiO2
Southern ENA (This study)
Newark Basin (This study)
Southern ENA
Northern ENA
Sierra Leone (This study)
Sierra Leone
Morocco (This study)
European CAMP
African CAMP
South American CAMP

Figure 3.

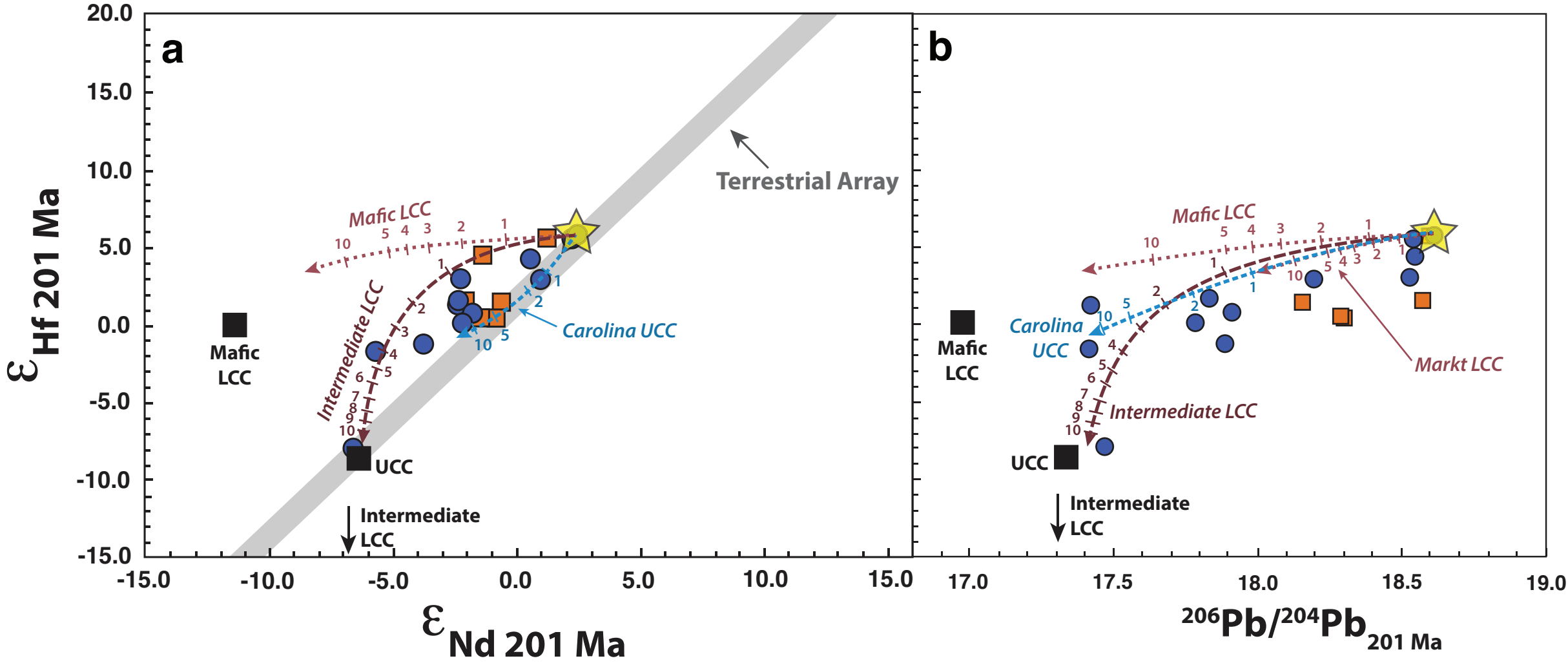
a
b
Terrestrial Array
Mafic LCC
Intermediate LCC
Carolina UCC
Markt LCC
Mafic LCC
UCC
Intermediate LCC
$\varepsilon_{Hf\ 201\ Ma}$
$\varepsilon_{Nd\ 201\ Ma}$
$^{206}Pb/^{204}Pb_{201\ Ma}$
20.0
15.0
10.0
5.0
0.0
-5.0
-10.0
-15.0
17.0
17.5
18.0
18.5
19.0

Figure 4.

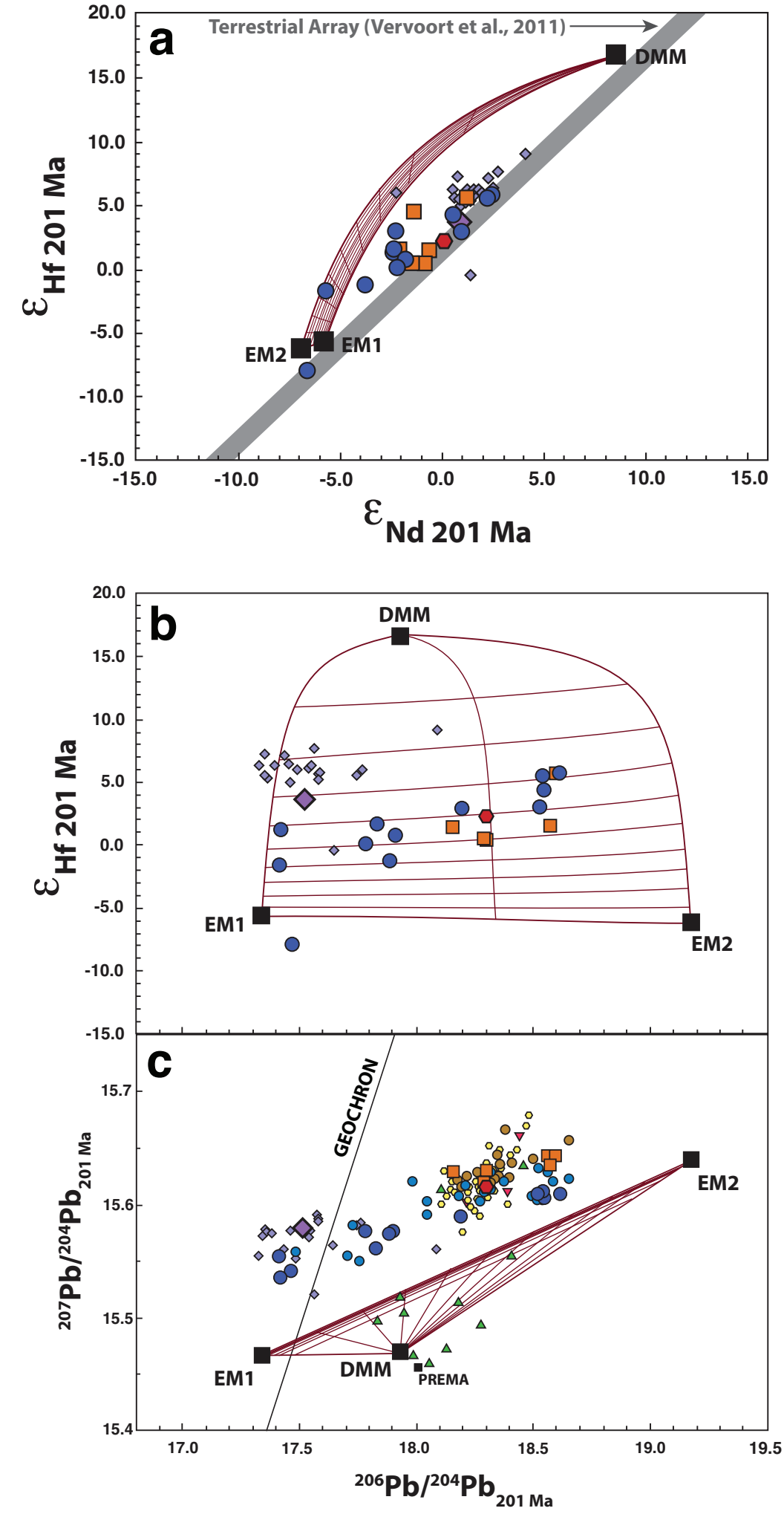
a
Terrestrial Array (Vervoort et al., 2011)
DMM
EM2
EM1
$\varepsilon_{Hf\ 201\ Ma}$
$\varepsilon_{Nd\ 201\ Ma}$
b
DMM
EM1
EM2
$\varepsilon_{Hf\ 201\ Ma}$
c
GEOCHRON
EM2
EM1
DMM
PREMA
$^{207}Pb/^{204}Pb_{201\ Ma}$
$^{206}Pb/^{204}Pb_{201\ Ma}$

Figure 5.

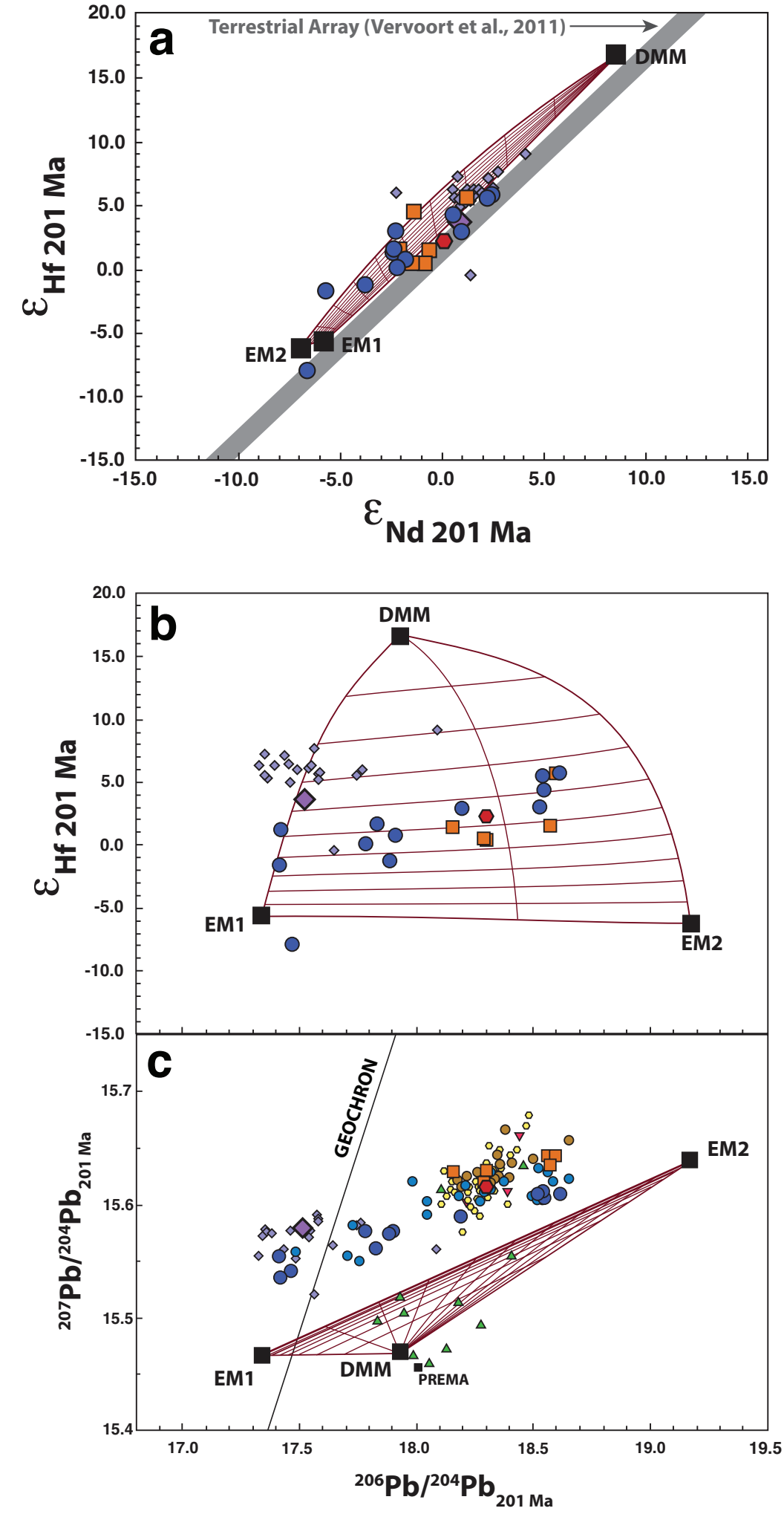
a
Terrestrial Array (Vervoort et al., 2011)
DMM
EM2
EM1
$\varepsilon_{Hf\ 201\ Ma}$
$\varepsilon_{Nd\ 201\ Ma}$
b
DMM
EM1
EM2
$\varepsilon_{Hf\ 201\ Ma}$
c
GEOCHRON
EM2
EM1
DMM
PREMA
$^{207}Pb/^{204}Pb_{201\ Ma}$
$^{206}Pb/^{204}Pb_{201\ Ma}$

Figure 6.

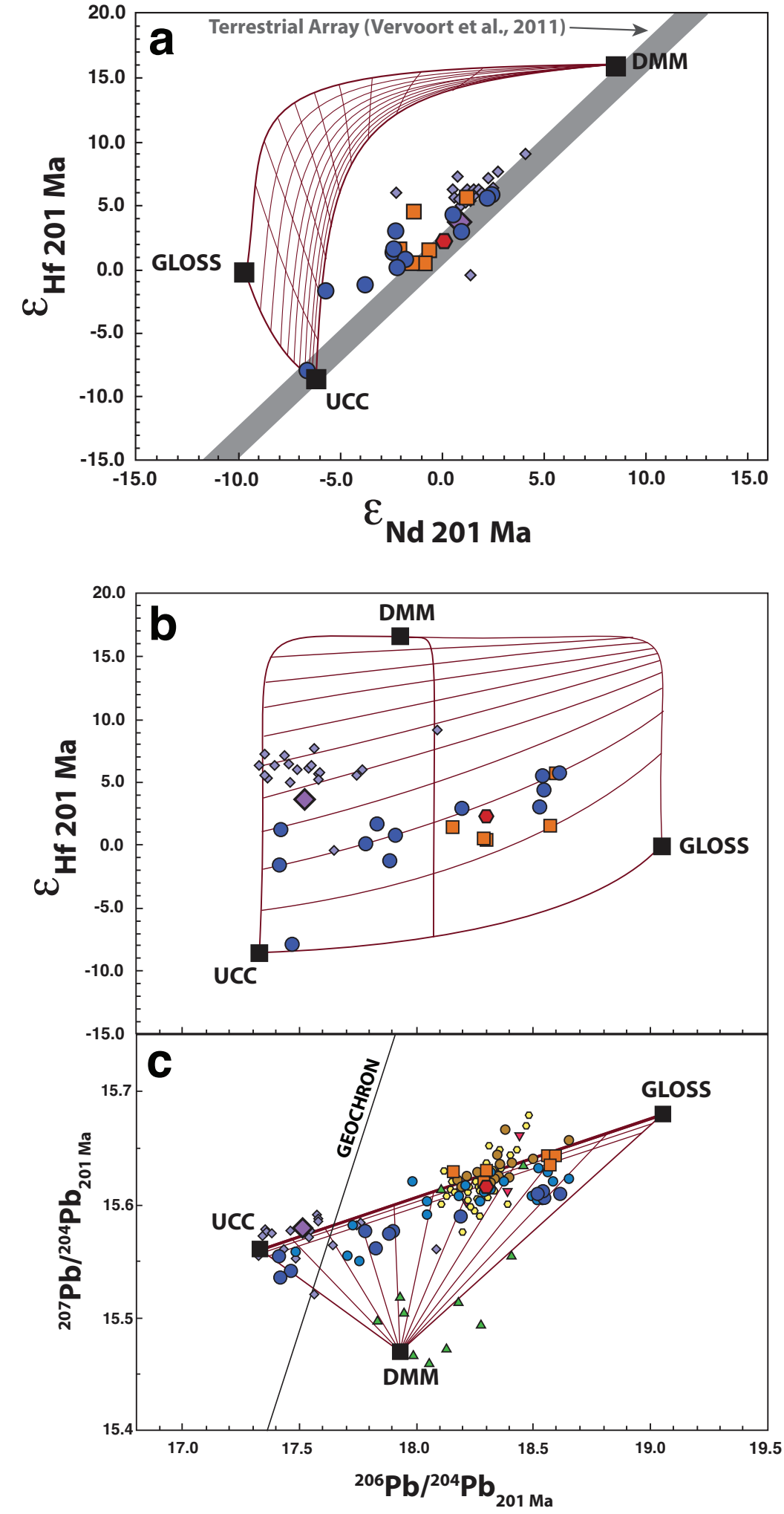
a
Terrestrial Array (Vervoort et al., 2011)
DMM
GLOSS
UCC
$\varepsilon_{Hf\ 201\ Ma}$
$\varepsilon_{Nd\ 201\ Ma}$
b
DMM
GLOSS
UCC
$\varepsilon_{Hf\ 201\ Ma}$
c
GEOCHRON
GLOSS
UCC
DMM
$^{207}Pb/^{204}Pb_{201\ Ma}$
$^{206}Pb/^{204}Pb_{201\ Ma}$

Figure 7.

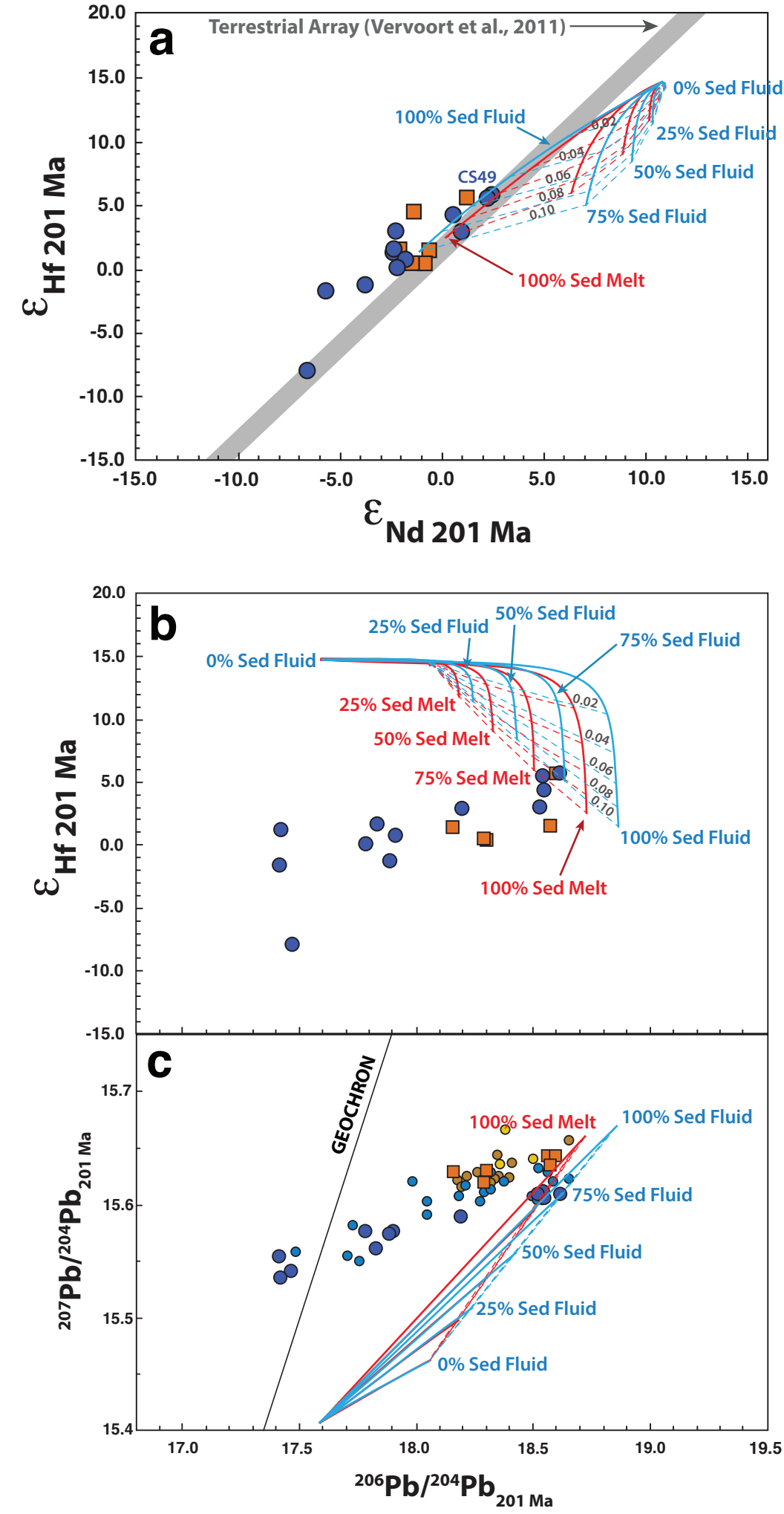
a
Terrestrial Array (Vervoort et al., 2011)
0% Sed Fluid
25% Sed Fluid
50% Sed Fluid
75% Sed Fluid
100% Sed Fluid
100% Sed Melt
CS49
0.02
0.04
0.06
0.08
0.10
εHf 201 Ma
εNd 201 Ma
b
0% Sed Fluid
25% Sed Fluid
50% Sed Fluid
75% Sed Fluid
100% Sed Fluid
25% Sed Melt
50% Sed Melt
75% Sed Melt
100% Sed Melt
εHf 201 Ma
c
GEOCHRON
100% Sed Melt
100% Sed Fluid
75% Sed Fluid
50% Sed Fluid
25% Sed Fluid
0% Sed Fluid
207Pb/204Pb201 Ma
206Pb/204Pb201 Ma

Figure 8.

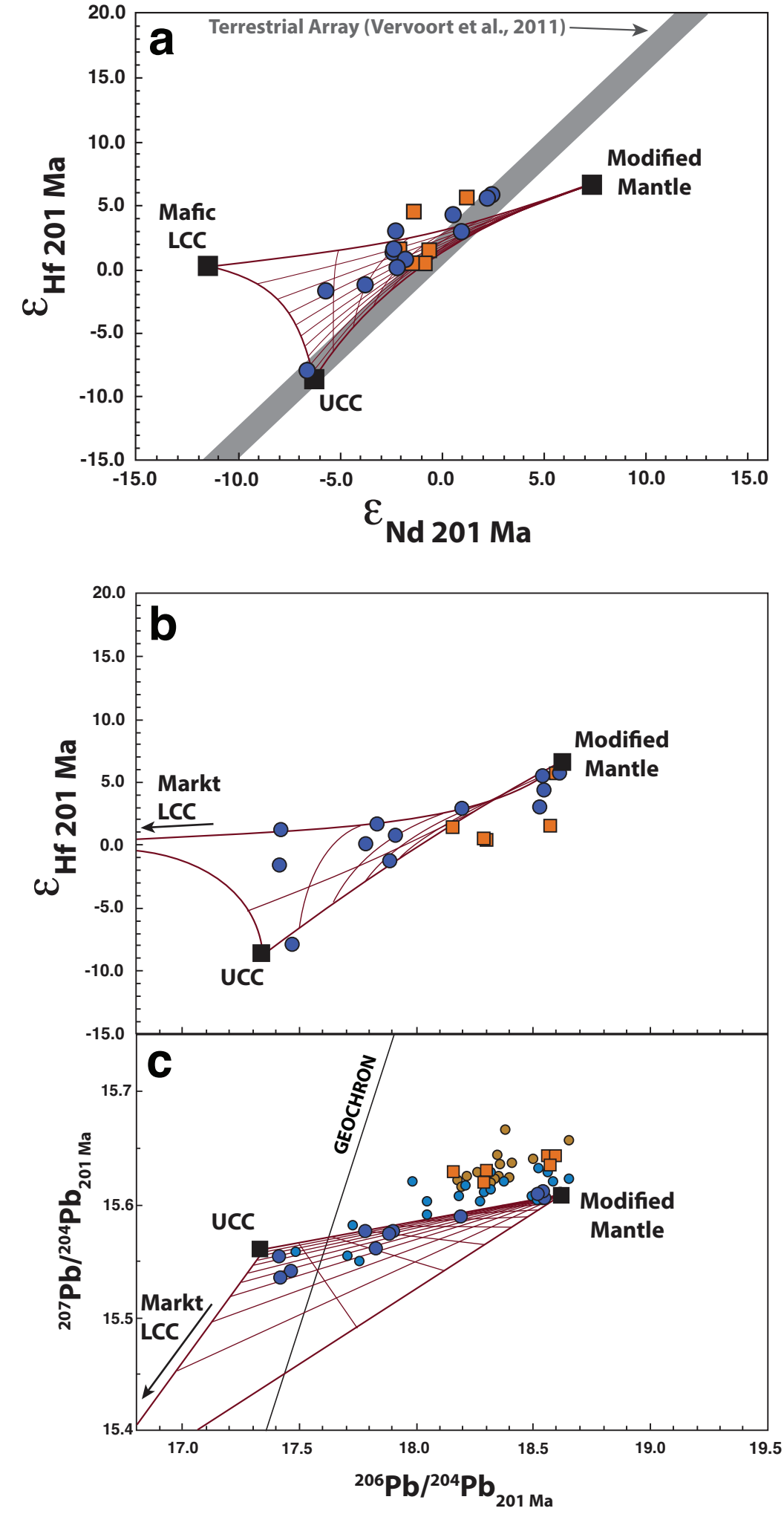
a
Terrestrial Array (Vervoort et al., 2011)
Modified Mantle
Mafic LCC
UCC
$\varepsilon_{Hf\ 201\ Ma}$
$\varepsilon_{Nd\ 201\ Ma}$
b
Modified Mantle
Markt LCC
UCC
$\varepsilon_{Hf\ 201\ Ma}$
c
GEOCHRON
UCC
Modified Mantle
Markt LCC
$^{207}Pb/^{204}Pb_{201\ Ma}$
$^{206}Pb/^{204}Pb_{201\ Ma}$

Table 1. Locations and characteristics of samples analyzed for this study, where available.

Sample name	Location description	Latitude (ºN)	Longitude (ºW)	Outcrop	Reference
Carolinas and Southern ENA:					
CS9	Georgia	34º 45' 21"	83º 29' 33"	Dike	Callegaro et al., 2013
CS26	South Carolina	34º 12' 27"	81º 03' 13"	Dike	Callegaro et al., 2013
CS23	South Carolina	34º 38' 53"	80º 31' 02"	Dike	Callegaro et al., 2013
CS28	South Carolina	34º 39' 08"	80º 31' 01"	Dike	Callegaro et al., 2013
CS14	South Carolina	34º 39' 27"	82º 01' 56"	Dike	Callegaro et al., 2013
CS41	North Carolina	34º 56' 14"	79º 49' 15"	Dike	Callegaro et al., 2013
CS48	North Carolina	35º 04' 15"	79º 50' 38"	Dike	Callegaro et al., 2013
CS46	North Carolina	35º 06' 48"	79º 48' 15"	Dike	Callegaro et al., 2013
CS55	North Carolina	35º 45' 48"	79º 02' 47"	Dike	Callegaro et al., 2013
CS57	North Carolina	35º 50' 11"	79º 00' 48"	Dike	Callegaro et al., 2013
CS49	North Carolina	36º 06' 47"	78º 46' 02"	Sill	Callegaro et al., 2013
CS73	Virginia	37º 17' 44"	78º 27' 38"	Dike	Callegaro et al., 2013
Newark basin:					
NEW03	Palisades Sill			Sill	Merle et al., 2014
NEW136C	Palisades Sill, olivine cumulate layer			Sill	Merle et al., 2014
NEW133	Orange Mountain flow	40º 18' 53"	75º 50' 53"	Lava Flow	Merle et al., 2014
NEW68	Preakness flow	40º 38' 50"	74º 34' 23"	Lava Flow	Merle et al., 2014
NEW52	Preakness flow	40º 40' 33"	74º 24' 32"	Lava Flow	Merle et al., 2014
NEW74	Hook Mountain flow	40º 49' 03"	74º 19' 45"	Lava Flow	Merle et al., 2014
Morocco:					
AN134	Tiourjdal section, basal flow	31° 07' 40"	7° 20' 46"	Lava Flow	Marzoli et al., 2004
Sierra Leone:					
SL45	High-TiO_2 sample, Freetown Layered Complex, Sierra Leone				Callegaro et al., 2017

Table 2. Hafnium isotope measurements for samples analyzed in this study.

Sample name	Lu (ppm) *	Hf (ppm) *	$^{176}Hf/^{177}Hf$	2σ **	ε_{Hf} [a]	$^{176}Hf/^{177}Hf_{201\ Ma}$	$\varepsilon_{Hf,\ 201\ Ma}$ [a]
Carolinas and Southern ENA:							
CS9	0.51	2.02	0.282879	0.000004	3.34	0.282745	3.02
CS26	0.45	1.61	0.282762	0.000004	-0.81	0.282613	-1.64
CS23	0.40	1.68	0.282908	0.000004	4.33	0.282782	4.33
CS28	0.35	1.17	0.282839	0.000003	1.93	0.282683	0.83
CS14	0.42	1.77	0.282753	0.000004	-1.14	0.282626	-1.16
CS41	0.32	0.94	0.282880	0.000004	3.35	0.282698	1.35
CS48	0.35	1.13	0.282826	0.000003	1.47	0.282664	0.17
CS46	0.43	2.54	0.282835	0.000004	1.76	0.282745	3.03
CS55	0.47	1.74	0.282960	0.000002	6.20	0.282818	5.62
CS57	0.37	1.11	0.282883	0.000004	3.46	0.282706	1.65
CS49	0.34	1.33	0.282962	0.000003	6.26	0.282825	5.86
CS73	0.38	1.54	0.282568	0.000003	-7.67	0.282437	-7.85
Newark basin:							
NEW03	0.29	2.95	0.282727	0.000002	-2.06	0.282674	0.53
NEW136C	0.20	1.54	0.282743	0.000004	-1.47	0.282673	0.50
NEW133	0.23	2.37	0.282754	0.000002	-1.11	0.282702	1.50
NEW68	0.25	2.22	0.282849	0.000002	2.26	0.282789	4.57
NEW52	0.35	2.07	0.282794	0.000004	0.32	0.282704	1.58
NEW74	0.62	3.00	0.282930	0.000002	5.13	0.282821	5.71
Morocco:							
AN134	0.31	3.66	0.282769	0.000002	-0.57	0.282724	2.27
Sierra Leone:							
SL45	0.05	0.16	0.282917	0.000005	4.67	0.282785	4.45

* Lutetium and Hf elemental compositions from Callegaro et al. (2013, 2017), Marzoli et al. (2004), and Merle et al. (2013).

** Uncertainties for $^{176}Hf/^{177}Hf$ measurements reported as 2σ standard errors.

[a] ε_{Hf} values for measured results calculated using a CHUR $^{176}Hf/^{177}Hf$ ratio of 0.282785. Age-corrected ε_{Hf} values for 201 Ma were calculated using an adjusted CHUR $^{176}Hf/^{177}Hf$ ratio of 0.282659.

Geochemistry Geophysics Geosystems

Supporting Information for

Assessing origins of end-Triassic tholeiites from Eastern North America using hafnium isotopes

Lynne J. Elkins[1, *], Christine M. Meyzen[2], Sara Callegaro[3], Andrea Marzoli[2], Michael Bizimis[4]

[1] University of Nebraska-Lincoln, Lincoln, NE 68510; lelkins@unl.edu

[2] Dipartimento di Geoscienze, Università degli Studi di Padova, Via G. Gradenigo, 6, 35131 Padova, Italy; andrea.marzoli@unipd.it, christine.meyzen@unipd.it

[3] Centre for Earth Evolution and Dynamics, University of Oslo, Oslo, Norway; sara.callegaro@geo.uio.no

[4] University of South Carolina; mbizimis@geol.sc.edu

Contents of this file

Additional Supporting Information (Files uploaded separately)

Introduction

The Supporting Information for this manuscript includes supporting figures showing trace element and isotope compositions for samples from this study. It also includes three supporting tables with modeling parameters for all of the calculations and models described in the main text. An additional supporting table, Table S4, is the

metasomatized mantle evolution model calculator from this study, provided as a user-enabled spreadsheet.

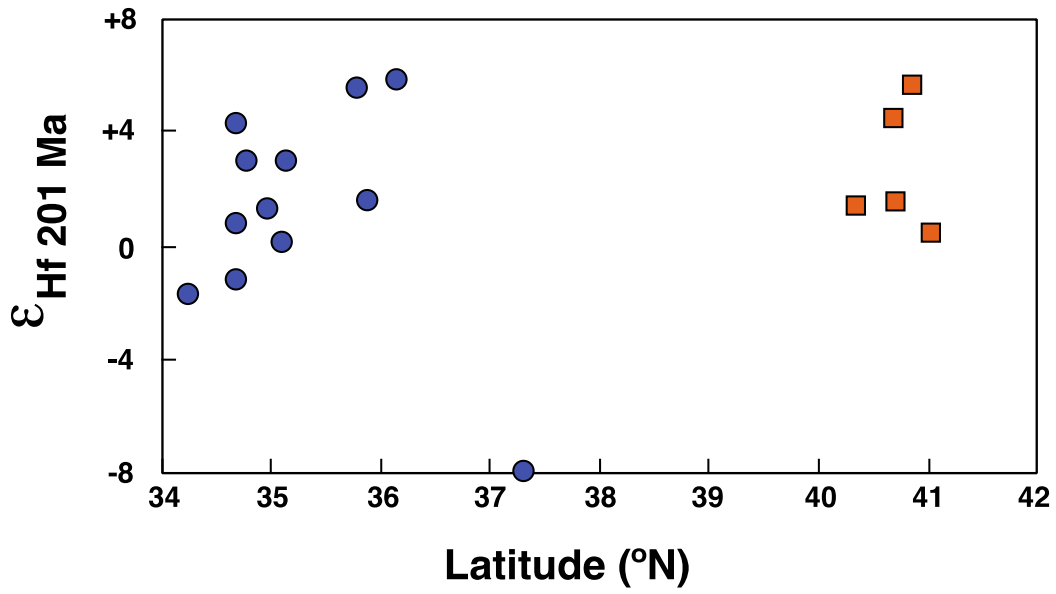

Figure S1. Age-corrected ε_{Hf} vs. latitude for ENA tholeiites from this study, including samples from the southern ENA region and the northern Newark basin. All symbols as in Figure 2.

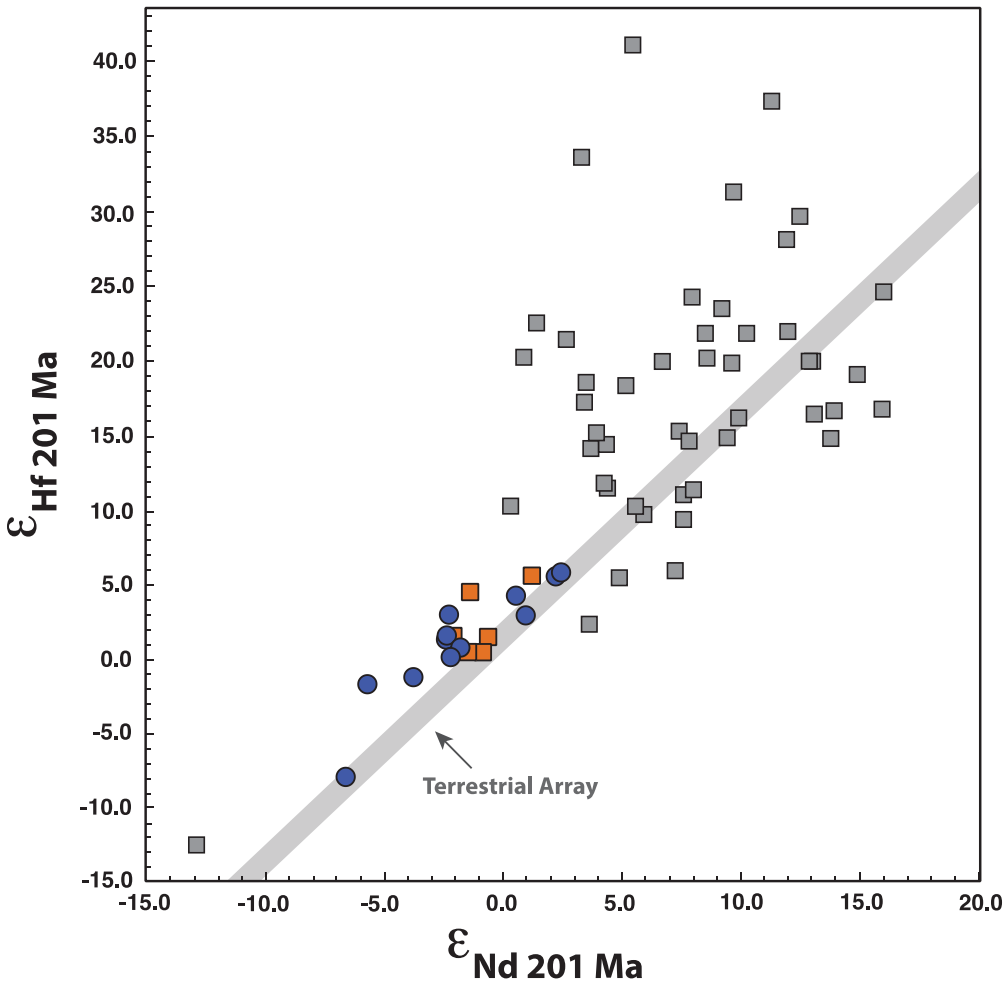

Figure S2. ε_{Hf} vs. ε_{Nd} showing samples from this study (symbols as in Figure 2) with globally representative SCLM-derived xenolith samples from Jordan, China, Morocco, and France (Choi et al., 2008; Shaw et al., 2007; Wittig et al., 2010) (gray squares).

	Lu (ppm)	Hf (ppm)	Sm (ppm)	Nd (ppm)	U (ppm)	Pb (ppm)	ε_{Hf}	$\varepsilon_{Hf,201\ Ma}$ [a]	ε_{Nd}	$\varepsilon_{Nd,201\ Ma}$ [b]	$\frac{^{206}Pb}{^{204}Pb}$	$\frac{^{206}Pb}{^{204}Pb_{201\ Ma}}$ [c]	$\frac{^{207}Pb}{^{204}Pb}$	$\frac{^{207}Pb}{^{204}Pb_{201\ Ma}}$ [d]	References
DMM solid source	0.63	0.20	0.27	0.71	0.005	0.023	+18.2	+16.7	+9.4	+8.5	-	-	-	-	Salters & Stracke, 2004; Klein et al., 2004
DMM partial melt (MORB)	-	2.9	-	6.1	-	0.2	+18.2	+16.7	+9.4	+8.5	-	-	-	-	
DMM alternate composition							+16.8	+14.3	+9.8	+8.4	18.28	17.93	15.49	15.47	Workman & Hart, 2005
EM1 solid source	0.1	0.4	0.54	1.67	0.04	0.23	-5.8	-5.7	-5.8	-5.8	17.77	17.34	15.49	15.47	Eisele et al., 2002; Jackson & Dasgupta, 2008; Willbold & Stracke, 2006; Woodhead & Devey, 1993
EM1 partial melt	-	9.3	-	60.0	-	5.5	-5.8	-5.7	-5.8	-5.8	17.77	17.34	15.49	15.47	
EM2 solid source	0.1	0.4	0.53	1.55	0.02	0.1	-5.9	-6.1	-6.6	-6.9	19.56	19.17	15.66	15.64	Jackson & Dasgupta, 2008; Jackson et al., 2007; Salters et al., 2011; Willbold & Stracke, 2006; Workman et al., 2004
EM2 partial melt	-	5.6	-	42.3	-	6.6	-5.9	-6.1	-6.6	-6.9	19.56	19.17	15.66	15.64	
Upper continental crust:															
Carolina terrane	-	2.0	-	65.0	-	25.9	-	-8.6 [e]	-	-6.3	-	17.4	-	15.6	Whalen et al., 2015, and references therein
Lower continental crust:															
Michigan mafic granulite	0.27	1.2	2.1	9.0	0.12	3.3	-0.2	+0.14	-13.0	-11.4	17.74	17.67	15.71	15.70	Zartman et al., 2013
Markt mafic granulite	-	-	-	-	0.5	2.5	-	-	-	-	16.9	16.5	15.4	15.3	Huang et al., 1995
Intermediate granulite	0.79	20.0	33.4	131.0	-	-	-21.5	-17.0	-13.0	-7.1	-	-	-	-	Schmitz et al., 2004
Average subducted sediment (GLOSS) [f]	0.41	4.06	5.80	27.0	1.68	19.9	+2.0	-0.07	-8.8	-9.67	18.91	19.1	15.67	15.68	Plank and Langmuir, 1998; Chauvel et al., 2008

[a] $^{176}Hf/^{177}Hf$ isotope ratios corrected to an age of 201 Ma using a ^{176}Lu decay constant of 1.867 x 10^{-11} a^{-1} (Söderland et al., 2004). ε_{Hf} values were determined using an age-corrected CHUR value of $^{176}Hf/^{177}Hf = 0.282659$, calculated using present-day CHUR values of $^{176}Hf/^{177}Hf = 0.282785$ and $^{176}Lu/^{177}Hf = 0.0336$ (Bouvier et al., 2008).

[b] $^{143}Nd/^{144}Nd$ isotope ratios corrected to an age of 201 Ma using a ^{147}Sm decay constant of 6.539 x 10^{-12} a^{-1} (Begemann et al., 2001). ε_{Nd} values were determined using an age-corrected CHUR value of $^{143}Nd/^{144}Nd = 0.512374$, calculated using present-day values of $^{143}Nd/^{144}Nd = 0.51263$ and $^{147}Sm/^{144}Nd = 0.196$ (Bouvier et al., 2008).

[c] $^{206}Pb/^{204}Pb$ isotope ratios corrected to 201 Ma using a ^{238}U decay constant of 1.551 x 10^{-10} a^{-1} (Jaffey et al., 1971).

[d] $^{207}Pb/^{204}Pb$ isotope ratios corrected to 201 Ma using a ^{235}U decay constant of 9.8485 x 10^{-10} a^{-1} (Jaffey et al., 1971).

[e] ε_{Hf} for Carolina terrane upper crust was calculated using the age-corrected ε_{Nd} value shown and the average terrestrial array best fit relationship after Vervoort et al. (2011).

[f] Subducted sediment isotope values determined using average subducted sediment compositions (GLOSS) with a calculated age of 170 Ma, chosen to represent subducted Paleozoic sediments in the CAMP melt region (i.e., sediments subducted around 370 Ma and later sampled by CAMP melting at 201 Ma), after Merle et al. (2011).

Table S1. Composition of source reservoirs and partial melts used for mixing and EC-AFC calculations.

Parameter [a]	Magma	Mafic LCC	Intermediate LCC	UCC	Units
$T_{liquidus}$	1380	1100	1000	1000	ºC
$T_{initial}$	1380	600	600	300	ºC
$T_{solidus}$	-	950	850	700	ºC
$T_{equilibrium}$	1100	1100	1100	1100	ºC
C_p	1484	1388	1380	1370	J/kg K
$H_{crystallization}$	396,000	-	-	-	J/kg
H_{fusion}	-	350,000	300,000	270,000	J/kg
D_{Hf} [b,c,d]	0.05	0.14	1.23	0.05	
D_{Nd}	0.04	0.14	0.17	0.09	
D_{Pb}	0.002	0.14	0.14	0.2	

[a] Liquidus and solidus temperatures, specific heat (C_p) values, and enthalpies estimated using values after Callegaro et al. (2017), Heinonen et al. (2016), and Bohrson and Spera (2001).

[b] Magmatic partition coefficients were determined using mineral/melt partition coefficients by McKenzie and O'Nions (1991) and fertile spinel peridotite modes of 60% olivine, 20% clinopyroxene, and 20% orthopyroxene.

[c] Mafic lower crust assimilant partition coefficients were determined using lower crustal granulite mineral modes after Zartman et al. (2013) and mineral/melt partition coefficients estimated from ranges compiled in the GERM Earthref catalog. Intermediate lower crust assimilant partition coefficients were determined for a granulite with 14% quartz, 42% garnet, 34% plagioclase, 3% clinopyroxene, 0.1% apatite, 0.1% zircon, and 1% rutile. This composition is comparable to intermediate granulite xenoliths measured by Schmitz et al. (2004) and Zartman et al. (2013). In the absence of accessory minerals, $D_{Hf} = 0.12$, $D_{Nd} = 0.10$, and $D_{Pb} = 0.13$.

[d] Upper crust assimilant partition coefficients were determined using average upper crust compositions after Taylor and Maclennan (1995) and Wedepohl (1995), which were used to calculate a stable upper crustal assemblage of 21% clinopyroxene, 38% quartz, 4% muscovite, 9% orthoclase, and 28% plagoclase; and mineral/melt partition coefficients estimated from ranges compiled in the GERM Earthref catalog.

Table S2. Model parameters used for EC-AFC calculations, after Bohrson and Spera (2001) and Spera and Bohrson (2001).

Table S3. Model parameters used for calculating the composition of residual metasomatized mantle (see Table S4).

	U	Th	Pb	Rb	Sr	Sm	Nd	Lu	Hf	References
DMM	0.005	0.01	0.02	0.09	9.8	0.3	0.7	0.06	0.2	Salters & Stracke, 2004
GLOSS	1.7	6.9	19.9	57.2	327	5.8	27	0.4	4.1	Plank & Langmuir, 1998
Altered Ocean Crust (AOC)	0.3	0.01	0.7	13	180	2.6	6.7	0.4	1.9	Staudigel et al., 1996
Partition coefficients, D_i:										
Bulk peridotite/melt [a]	0.0065	0.0044	0.0012	0.0012	0.0071	0.041	0.020	0.61	0.065	McKenzie & O'Nions, 1991; Salters et al., 2002
Bulk sediment/melt [b]	1.0	1.2	1.0	1.1	0.6	2.9	3.0	5.5	2.4	Johnson & Plank, 2000
Bulk sediment/fluid [c]	3.1	4.5	0.8	1.7	0.7	2.0	2.4	2.5	2.1	Johnson & Plank, 2000
AOC Mobility coefficients [d]	0.3	0.4	0.9	0.6	0.4	0.1	0.31	0.01	0.01	Kogiso et al., 1997

	$\frac{^{206}Pb}{^{204}Pb}$	$\frac{^{207}Pb}{^{204}Pb}$	$\frac{^{207}Pb}{^{204}Pb}$	$\frac{^{87}Sr}{^{86}Sr}$	$\frac{^{143}Nd}{^{144}Nd}$	$\frac{^{176}Hf}{^{177}Hf}$	References
DMM	18.4	15.5	37.8	0.70254	0.51315	0.28317	Salters & Stracke, 2004
GLOSS	18.9	15.7	38.9	0.7173	0.51218	0.2824	Plank & Langmuir, 1998
Altered Ocean Crust (AOC) [e]	18.4	15.5	37.8	0.70458	0.51308	0.28320	Salters & Stracke, 2004; Staudigel et al., 1996

[a] Peridotite/melt partition coefficients were calculated using a fertile garnet peridotite composition with 59% olivine, 8% clinopyroxene, 21% orthopyroxene, and 12% garnet. Mineral/melt partition coefficients were drawn from experiments RD1097-1 and RD1097-5 of Salters et al. (2002) and calculated values of McKenzie and O'Nions (1991).

[b] Sediment/melt partition coefficients are averaged from experiments PC 36 and PC 39 of Johnson and Plank (2000).

[c] Sediment/fluid partition coefficients are averaged from experiments PC 38 and PC 47 of Johnson and Plank (2000).

[d] Mobility coefficients for AOC are shown as percent mobilities, after Kogiso et al (1997).

[e] Trace element concentrations for AOC are derived from Atlantic drilling site 417/418 (Staudigel et al., 1996).

Table S4. Metasomatized mantle evolution calculator (download as .xlsx file).